NASA/CR—2013-216527

Multiphase Transport in Porous Media: Gas-Liquid Separation Using Capillary Pressure Gradients

International Space Station (ISS) Flight Experiment Development Final Report

Richard R. Wheeler, Jr., John T. Holtsnider, Roger W. Dahl, and Dalton Deeks
UMPQUA Research Company, Myrtle Creek, Oregon

Goran N. Jovanovic, James M. Parker, and Jim Ehlert
J-Lab and Associates, Tigard, Oregon

August 2013

NASA STI Program . . . in Profile

Since its founding, NASA has been dedicated to the advancement of aeronautics and space science. The NASA Scientific and Technical Information (STI) program plays a key part in helping NASA maintain this important role.

The NASA STI Program operates under the auspices of the Agency Chief Information Officer. It collects, organizes, provides for archiving, and disseminates NASA's STI. The NASA STI program provides access to the NASA Aeronautics and Space Database and its public interface, the NASA Technical Reports Server, thus providing one of the largest collections of aeronautical and space science STI in the world. Results are published in both non-NASA channels and by NASA in the NASA STI Report Series, which includes the following report types:

- TECHNICAL PUBLICATION. Reports of completed research or a major significant phase of research that present the results of NASA programs and include extensive data or theoretical analysis. Includes compilations of significant scientific and technical data and information deemed to be of continuing reference value. NASA counterpart of peer-reviewed formal professional papers but has less stringent limitations on manuscript length and extent of graphic presentations.

- TECHNICAL MEMORANDUM. Scientific and technical findings that are preliminary or of specialized interest, e.g., quick release reports, working papers, and bibliographies that contain minimal annotation. Does not contain extensive analysis.

- CONTRACTOR REPORT. Scientific and technical findings by NASA-sponsored contractors and grantees.

- CONFERENCE PUBLICATION. Collected papers from scientific and technical conferences, symposia, seminars, or other meetings sponsored or cosponsored by NASA.

- SPECIAL PUBLICATION. Scientific, technical, or historical information from NASA programs, projects, and missions, often concerned with subjects having substantial public interest.

- TECHNICAL TRANSLATION. English-language translations of foreign scientific and technical material pertinent to NASA's mission.

Specialized services also include creating custom thesauri, building customized databases, organizing and publishing research results.

For more information about the NASA STI program, see the following:

- Access the NASA STI program home page at *http://www.sti.nasa.gov*

- E-mail your question to *help@sti.nasa.gov*

- Fax your question to the NASA STI Information Desk at 443–757–5803

- Phone the NASA STI Information Desk at 443–757–5802

- Write to:
  STI Information Desk
  NASA Center for AeroSpace Information
  7115 Standard Drive
  Hanover, MD 21076–1320

NASA/CR—2013-216527

Multiphase Transport in Porous Media: Gas-Liquid Separation Using Capillary Pressure Gradients

International Space Station (ISS) Flight Experiment Development Final Report

Richard R. Wheeler, Jr., John T. Holtsnider, Roger W. Dahl, and Dalton Deeks
UMPQUA Research Company, Myrtle Creek, Oregon

Goran N. Jovanovic, James M. Parker, and Jim Ehlert
J-Lab and Associates, Tigard, Oregon

Prepared under Grant NNX09AK64

National Aeronautics and
Space Administration

Glenn Research Center
Cleveland, Ohio 44135

August 2013

This report is a formal draft or working paper, intended to solicit comments and ideas from a technical peer group.

Level of Review: This material has been technically reviewed by NASA expert reviewer(s).

Available from

NASA Center for Aerospace Information
7115 Standard Drive
Hanover, MD 21076–1320

National Technical Information Service
5301 Shawnee Road
Alexandria, VA 22312

Available electronically at http://www.sti.nasa.gov

Abstract: Advances in the understanding of multiphase flow characteristics under variable gravity conditions will ultimately lead to improved and as of yet unknown process designs for advanced space missions. Such novel processes will be of paramount importance to the success of future manned space exploration as we venture into our solar system and beyond. In addition, because of the ubiquitous nature and vital importance of biological and environmental processes involving air/water mixtures, knowledge gained about fundamental interactions and the governing properties of these mixtures will clearly benefit the quality of life here on our home planet. The techniques addressed in the current research involving multiphase transport in porous media and gas-liquid phase separation using capillary pressure gradients are also a logical candidate for a future International Space Station (ISS) flight experiment. Importantly, the novel and potentially very accurate Lattice-Boltzmann (LB) modeling of multiphase transport in porous media developed in this work offers significantly improved predictions of real world fluid physics phenomena, thereby promoting advanced process designs for both space and terrestrial applications.

This 3-year research effort has culminated in the design and testing of a zero-g demonstration prototype. Both the hydrophilic (glass) and hydrophobic (Teflon) media Capillary Pressure Gradient (CPG) cartridges prepared during the second year's work were evaluated. Results obtained from ground testing at 1-g were compared to those obtained at reduced gravities spanning Martian (1/3-g), Lunar (1/6-g) and zero-g. These comparisons clearly demonstrate the relative strength of the CPG phenomena and the efficacy of its application to meet NASA's unique gas-liquid separation (GLS) requirements in non-terrestrial environments.

LB modeling software, developed concurrently with the zero-g test effort, was shown to accurately reproduce observed CPG driven gas-liquid separation phenomena. The design and fabrication of a micropost plate-lamina Hele-Shaw (HS) cell was performed which served as a computationally attainable geometric structure facilitating direct comparison between physical phenomena observed in our laboratory and the LB software predictions.

PROJECT DESCRIPTION.

Porous media occurs within various Life Support Systems aboard the Shuttle Orbiter and International Space Station, and will most probably occur in future Exploration Life Support (ELS) and In-Situ Resource Utilization (ISRU) systems to be developed for manned Lunar and Mars missions. One example of such a system is the Microbial Check Valve (MCV®). This flow-through cartridge contains spherical iodine impregnated polymer beads, which produce a contact microbial kill and impart an iodine residual to water to prevent microbial growth. MCV®s are used in various locations on the Shuttle to provide potable water for the crew. A related device containing similar iodinated media, the EMU bacterial filter, is used to prevent back-contamination of the Shuttle or ISS potable water supplies when sublimation cooling water is provided to the Portable Life Support System (PLSS) prior to EVA.

In another major system, the ISS Water Processor Assembly (WPA) utilizes Multifiltration (MF) beds which contain sequential layers of spherical anion- and cation-exchange resins, and amorphous granular activated carbon, which provide the first stage of chemical water purification following filtration of particulates. The next stage of water purification in the WPA occurs within the Volatile Removal Assembly (VRA), a three-phase (gas-liquid-solid), heterogeneous catalytic oxidation reactor that converts dissolved organics not removed by adsorption in the MF beds to CO_2 and carboxylic acids. This reactor contains a packed-catalyst bed consisting of noble metals dispersed on alumina support pellets through which liquid water and gas-phase O_2 flow at elevated temperature and pressure. Following gas-liquid separation (to remove product CO_2 and excess O_2), the water is post-treated using another bed containing a mixture of ion-exchange (IX) resin spheres. Here, the carboxylic acids and any other ionic contaminants are removed in the final water-polishing step, and elemental iodine is added via MCV® resin to ensure potability.

Packed beds of porous media are also employed for air purification. The ISS Carbon Dioxide Removal Assembly (CDRA) contains granular beds of two zeolites, Molecular Sieve 13X and Molecular Sieve 5A. The Trace Contaminant Control System (TCCS) removes volatile airborne contaminants by adsorption of ammonia and some

organics on a packed bed of phosphoric acid impregnated activated carbon. The remaining organics are destroyed in a high temperature catalytic reactor using a palladium catalyst supported on alumina. In addition, the ISS Oxygen Generation Assembly (OGA) replenishes atmospheric O_2 levels by electrolysis of water, which is first treated by passage through another MF bed of purification media. Significant to the present work, one of the team-members, Umpqua Research Company (URC), provides the MCVs®, multifiltration Unibeds®, EMU bacterial filters, VRA Post-treatment and OGA pre-treatment beds in support of the Shuttle and ISS programs.

Many advanced ELS technologies currently under development use packed catalyst or sorbent beds. These include Sabatier and Bosch reactors for recovery of oxygen from atmospheric CO_2, the Vapor Phase Catalytic Ammonia Removal (VPCAR) system which uses both catalytic oxidation and reduction reactors, and various forms of biological water processors. Future ISRU systems for recovery of O_2 from the lunar regolith or from the Martian atmosphere or CO_2 ice will also most probably employ packed catalyst beds.

Given the widespread employment of porous media in Life Support Systems, a more detailed understanding of multiphase flow phenomena will be very beneficial. For example, the VRA is intentionally a two-phase gas-liquid flow system. What happens to flow characteristics (and reactor efficiency) if the surface properties of the catalyst bed change over time due to the deposition of partially oxidized organics on the catalyst surface, resulting in partial shifting of wettability from strongly water-wet (hydrophilic) to partially hydrophobic or even strongly hydrophobic character? What happens in the WPS multifiltration beds or post-treatment IX beds, when gas leaks into the system during a malfunction or during change-out? What happens if liquid phase water enters into the gas-phase beds used for air purification? When anomalous behavior occurs, what is the best way to regain full operational capability? The experiments and the numerical simulation methods which we propose can be used to answer questions of this kind, and also to help develop new component designs to meet future needs.

The Lattice-Boltzmann (LB) modeling approach is naturally based on the local balance of mass, momentum, and energy content of fluid elements. Fluid elements are

envisioned as discretely distributed (imaginary) nodes, which exchange their energy and mass content with surrounding neighboring nodes. Since LB modeling is based on strictly localized phenomena, any macroscopic properties have to emanate from local mass, momentum, energy, and thermodynamic functional properties related to the local composition. This means that macroscopic properties (higher scale quantities) like surface tension, contact angle, and curvature of the interface have to be generated from the local state of the node and its corresponding thermodynamic functional properties. In other words, surface tension, contact angle, and curvature of the interface emerge as macroscopic consequences of the local "states" of fluid nodes rather than being introduced as independent variables. Parker and Jovanovic recently showed that an extended concept of the local chemical potential is sufficient to solve a multiphase flow model with accurate fluid-fluid and fluid-solid interface behavior[1-3]. While the local energy potential and mass composition determines the usual properties of the fluid (density, viscosity, equilibrium composition, etc.), the gradient of the energy potential among neighboring nodes is the key element in estimating all mass and energy transport phenomena. For example, the chemical potential (energy per unit volume of the fluid) of water at any fluid node is determined by temperature, pressure, and composition of all species present at the given node. The gradient of chemical potential of water among neighboring nodes will determine diffusional mass transfer of water, and local pressure gradients, which, if viewed macroscopically, qualitatively and quantitatively represent interfacial surface tension.

While the Lattice-Boltzmann method is based on fundamental kinetic-gas theory, at the continuum limit the LB method exactly solves problems that are typically described by Navier-Stokes equations, which include: viscous, inertial, pressure, and external body forces like gravity and buoyancy. It has been shown that superposition of all above-mentioned forces and phenomena is feasible within the realm of LB modeling. More importantly, LB modeling facilitates easy combination and/or exclusion of forces and phenomena, thus allowing simulation of cases which are difficult or impossible to realize experimentally. For example, one can easily simulate cases in microgravity and variable gravity (0-g, lunar-g, Martian-g) environments. In addition, it is very pertinent for the proposed study that Lattice-Boltzmann methods are able to simulate cases

where distributed geometrical characteristics like variable particle size distribution, and distributed intermolecular attractions on solid-liquid interfaces (i.e., variable contact angle) effectively result in macroscopic properties of porous media.

Significant progress in simulating interfacial interactions has been made by Professor Jovanovic's group at Oregon State University (OSU) by using LB techniques to model phase separation as a diffusive process driven by gradients of chemical potential[1-3]. By representing the driving forces for molecular diffusion in a thermodynamically consistent manner, the interfaces do not need to be explicitly tracked or captured, but will develop naturally in the system. In addition, in the modeling of multiphase processes like mixing, reactions, and separations, it is necessary that a model accurately represent the molecular composition of a multiphase system at all locations, both at interfaces and in the bulk. In this approach, it is possible to accurately describe the mass transfer, fluid flow, thermodynamic equilibrium, surface effects, and external field effects in a model.

The goal of our research is the development of hardware, methodology, and advanced numerical simulation capability to enable a series of International Space Station (ISS) microgravity experiments which will: (1) provide fundamental information on 2-phase gas-liquid transport in porous media in the absence of gravity, (2) demonstrate effective gas-liquid phase separation via the passive capillary pressure gradient approach[4-6], (3) validate the predictions of the numerical model, and, (4) convert the numerical model into a software design tool.

Ultimately we envision the construction of a modular apparatus, capable of mating directly with the ISS Fluids Integrated Rack. The apparatus will consist of pumps (if needed), air-water flow controllers, and a support frame which will provide the necessary fluid inlet and outlet connections, and will accept Hele-Shaw (HS) cell 'cartridges' which can be quickly inserted and withdrawn with a minimum of astronaut time and inconvenience. Each cartridge will correspond to a particular experiment. Geometrically, the Hele-Shaw cells will have dimensions determined from experimental results, numerical modeling, and guidance received from knowledgeable personnel within NASA. Means must be derived for effective 'docking' and leak-free mating of

these cartridges with the flow inputs and outputs supplied by the support frame. Minimum instrumentation would monitor differential pressure and provide flow measurements for influent and effluent lines.

1.0 EXPERIMENTAL PLAN AND PROTOTYPE DESIGN.

The experimental plan was to utilize flow-through cartridges, as depicted in Figure 1.1, fabricated to employ Capillary Pressure Gradient (CPG) phenomena, to demonstrate significant separation of air and water in a zero-g environment over a range of flow rates and gas-liquid feed ratios. In the absence of gravity, weak capillary forces, which form the base of operation for this technique, would be shown to dominate and effectively drive gas/liquid separation at (or scalable to) useful flow rates.

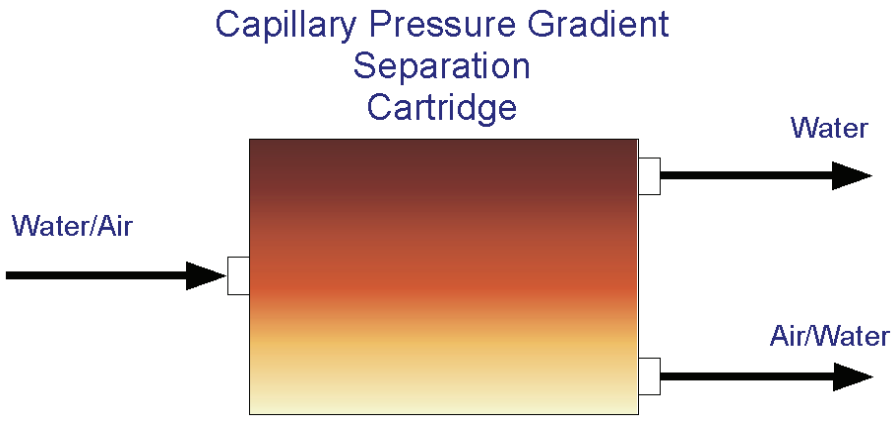

Figure 1.1. Representative CPG Cartridge with Vertical Gradation.

Three CPG cartridges were fabricated for this work. One was filled with glass media (hydrophilic), one was filled with Teflon media (hydrophobic), and one, a pin-plate design, was fabricated via photo-lithography and chemical etching to form pins on one side of a metal plate that was naturally hydrophilic. Due to both delays in fabrication and our experiment duration being limited to two flight days, only the glass media and Teflon media CPGs were flown. These media filled cartridges were fabricated, as shown in Figure 1.2, using glass plates that bound the front and back sides of the cartridge permitting the maximum visibility of gas-liquid separation (GLS) in the quasi two-dimensional cell. The combination of the magnitude of the media's hydrophobicity/

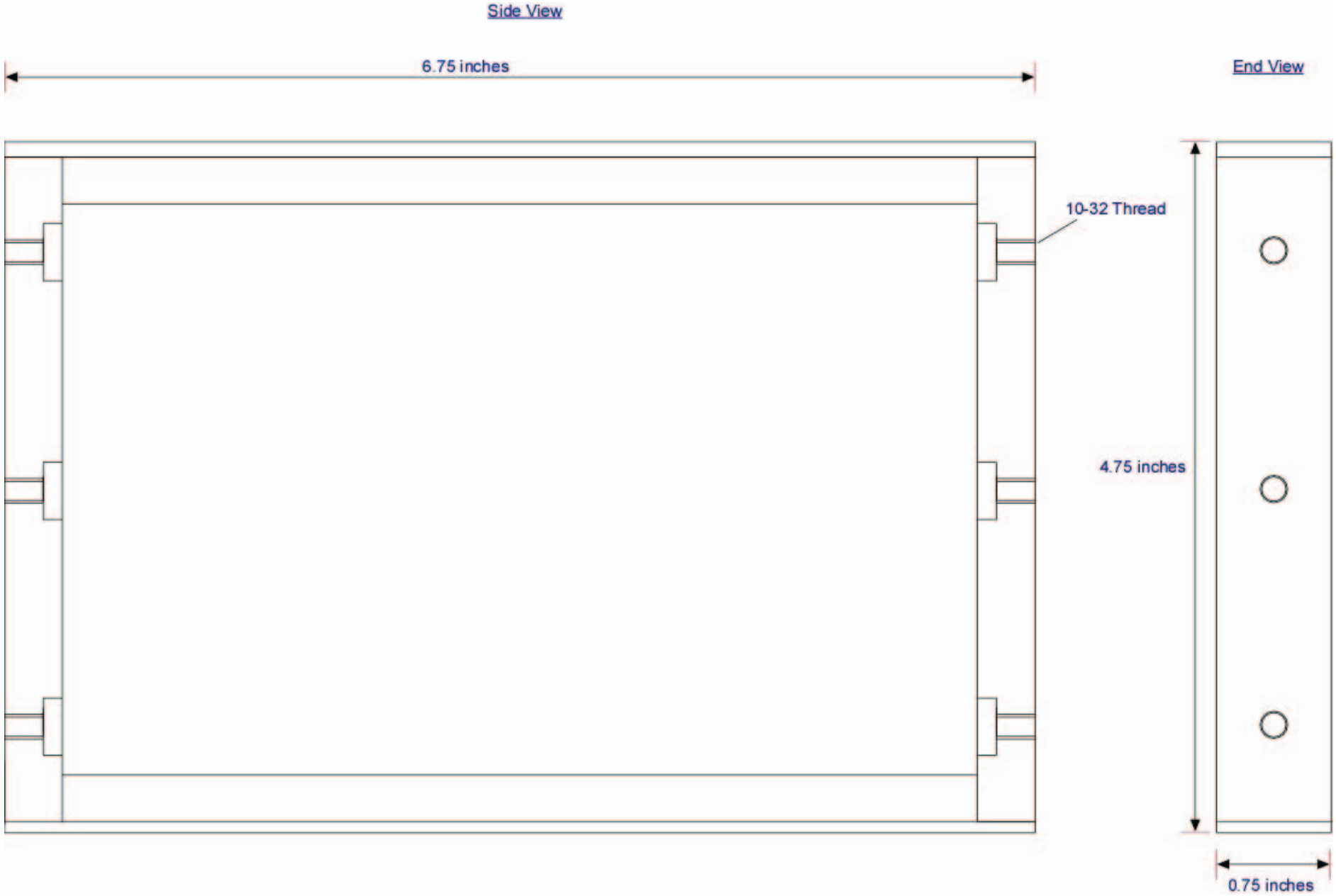

Figure 1.2. CPG Cartridge Schematic (6061 Aluminum body with 1/8 inch thick Plate Glass windows)

hydrophilicity and the vertically distributed (layered) particle size gradient directly determine the resulting capillary pressure gradient. At a sufficiently reduced gravity the resulting CPG force takes control and acts on gas-liquid interfaces to separate these fluid components contained in a mixed inlet stream into two separate outlet streams, one containing pure liquid and the other a concentrated gas-liquid mixture. For the current work, the outlet port to which the liquid flow is driven by the CPG forces is defined as the “upper” port while the “lower” port is defined as the port to which the gas component is driven. The reason for the “upper” and lower” port terminology arises from the implicit goal of this research to demonstrate gas liquid separation (for a vertically oriented cartridge) in opposition to the gravity induced buoyancy force which

Figure 1.3. Glass media (Top) and Teflon media (Bottom) CPG cartridges, each with a single mixed stream inlet port on the left hand side and the upper and lower outlet ports on the right hand side.

would, if acting alone, cause the gas component to be collected at the upper port. Figure 1.3 contains photos of the fabricated CPG cartridges.

For the experimental apparatus two multichannel peristaltic pumps were employed to allow the independently controlled delivery of gas and liquid to the CPG cartridge under test. Predetermined settings were utilized on each pump to provide known gas to liquid feed ratios as well as the total combined fluid flow rate. Multiple channels of water flow were connected in parallel with one or more channels of air flow. Flow of each fluid was determined by the pump speed setting as well as the number of channels and the size (inner diameter) of the peristaltic tubing used on each pump.

Flexible feed and collection bags were utilized to contain the air/water mixtures. Flexible bags rapidly equilibrate with the local environmental pressure and minimize the effects of environmental pressure fluctuations on pump throughput. A flexible feed bag containing only water provides minimal pressure head to the peristaltic pump. Air was pulled directly from the cabin and therefore did not require a separate feed bag. Flexible collection bags on each outlet channel provide minimal back pressure to the cartridge under test. These outlet bags were evacuated prior to experiment so as to minimize measured gas collection error.

A flow schematic for the experimental prototype is shown in Figure 1.4. Air and colored water are pulled through independent peristaltic pump heads and combined in a Tee fitting. This mixed air-water stream flows through a bypass valve to either a bypass collection bag or directly to the CPG cartridge inlet. Effluent from the CPG cartridge is collected in separate bags for both the upper and lower outlet ports. Quick disconnects were utilized throughout to permit easy inflight bag/cartridge replacement.

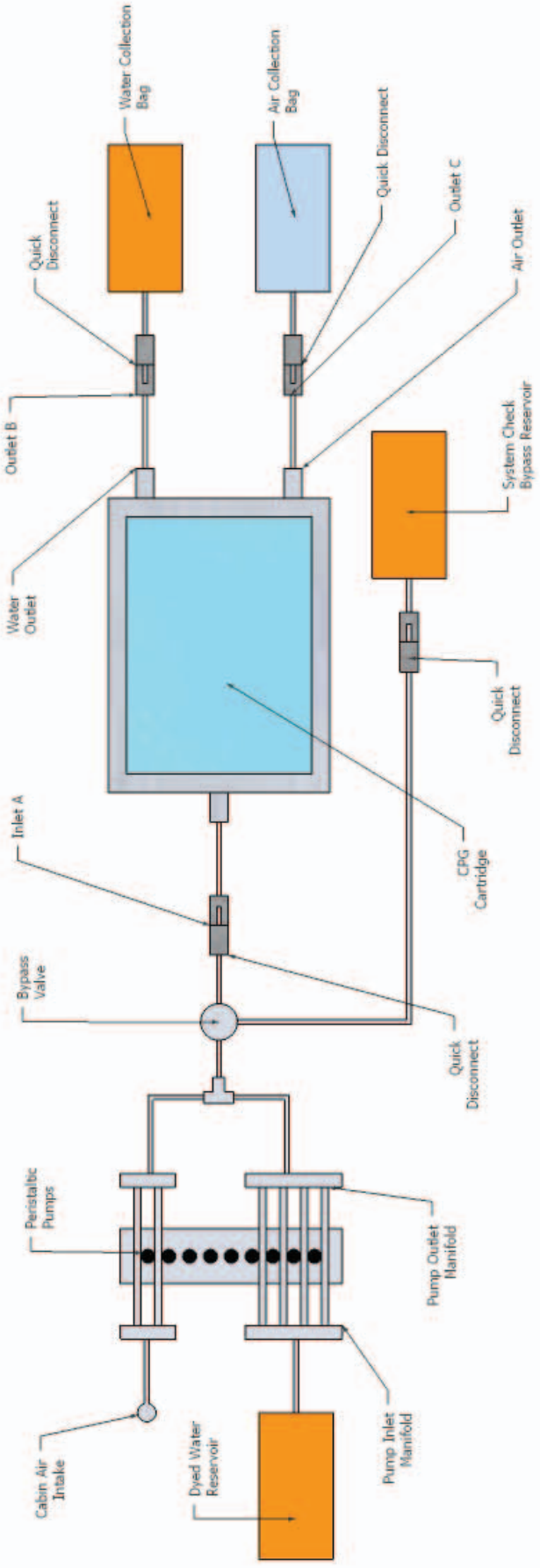

Figure 1.4. Prototype Flow Schematic.

Due to fluid volume requirements the water input reservoir must be replaced mid-flight by releasing the safety strap on the mount. The full input reservoir in the storage cooler was then swapped with the empty reservoir. The input bags were doubly contained in one gallon plastic jars for added protection against punctures and leaking. The 700 milliliter output bags were double contained in a sealed plastic box with quick-connects accessible on the outside. Fabric encased tubes of sorbent material were placed along the periphery of this box as an additional leak containment measure. The box was attached to the base plate with aluminum angles. Large washers backed the bolts within the box to reinforce the connection. A total of four input/bypass reservoirs and six liters of water were taken on each flight. One input reservoir containing three liters of water, one bypass reservoir for the time between zero-g parabolas, and eight empty output reservoirs were needed for each flight. Reserve reservoirs were stored in a cooler to be available in-flight if required. Photos and drawings of the equipment used and the prototype details are shown in Figures 1.5-1.8.

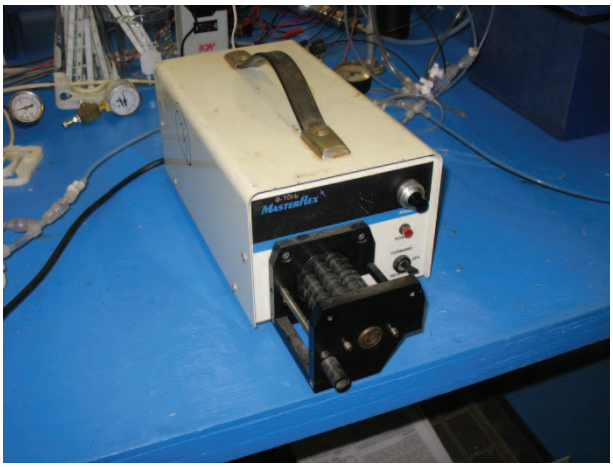

Figure 1.5. Masterflex 7520-35 Peristaltic Pump

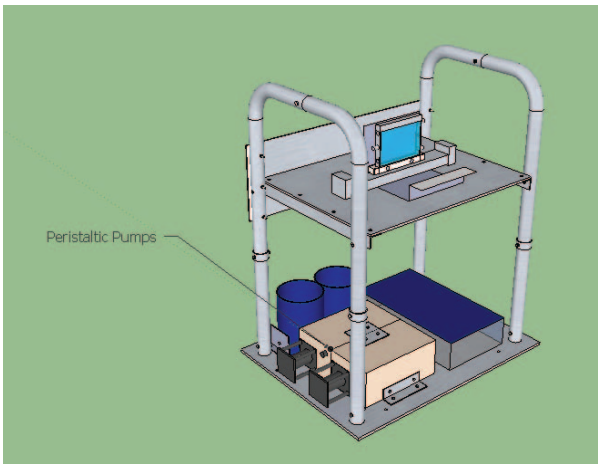

Figure 1.6. Pump Locations on Equipment Rack

Figure 1.7. Input/Bypass Reservoir (left), Output Reservoir (right)

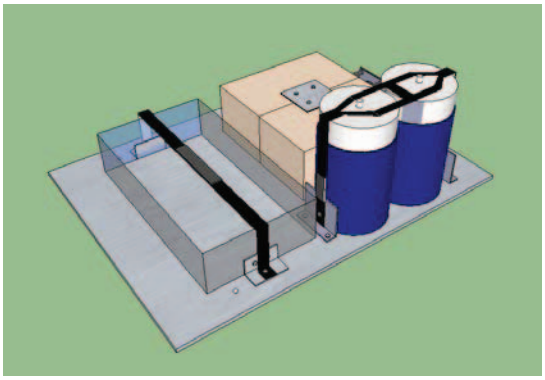

Figure 1.8. Reservoir Strapping

A Samsung WB210 High Definition (HD) video capable camera with good base resolution (14 Mpixel) allowed observation of the air/water phase boundary (bubble) progression at the inlet and outlets of the CPG cartridge. The use of colored water prepared using water soluble food dyes permitted improved air/water phase boundary contrast when viewed using adequate back-lighting provided by an LED matrix. A g-force indicator, comprised of a test-mass attached to a weak spring confined in a plastic syringe barrel was located in the lower front region of the camera's video frame permitting simultaneous gravity data recording. The entire CPG cartridge/backlighting/camera mount assembly is located on an pin-locked spindle that permits rotation of the entire assembly about its axis through 90 degrees between the vertical and horizontal positions. Schematics of the prototype with the CPG cartridge oriented vertically and horizontally are show in Figure 1.9. The camera (not shown in Figure 1.9) is located on the rotating shelf directly in front of the CPG cartridge.

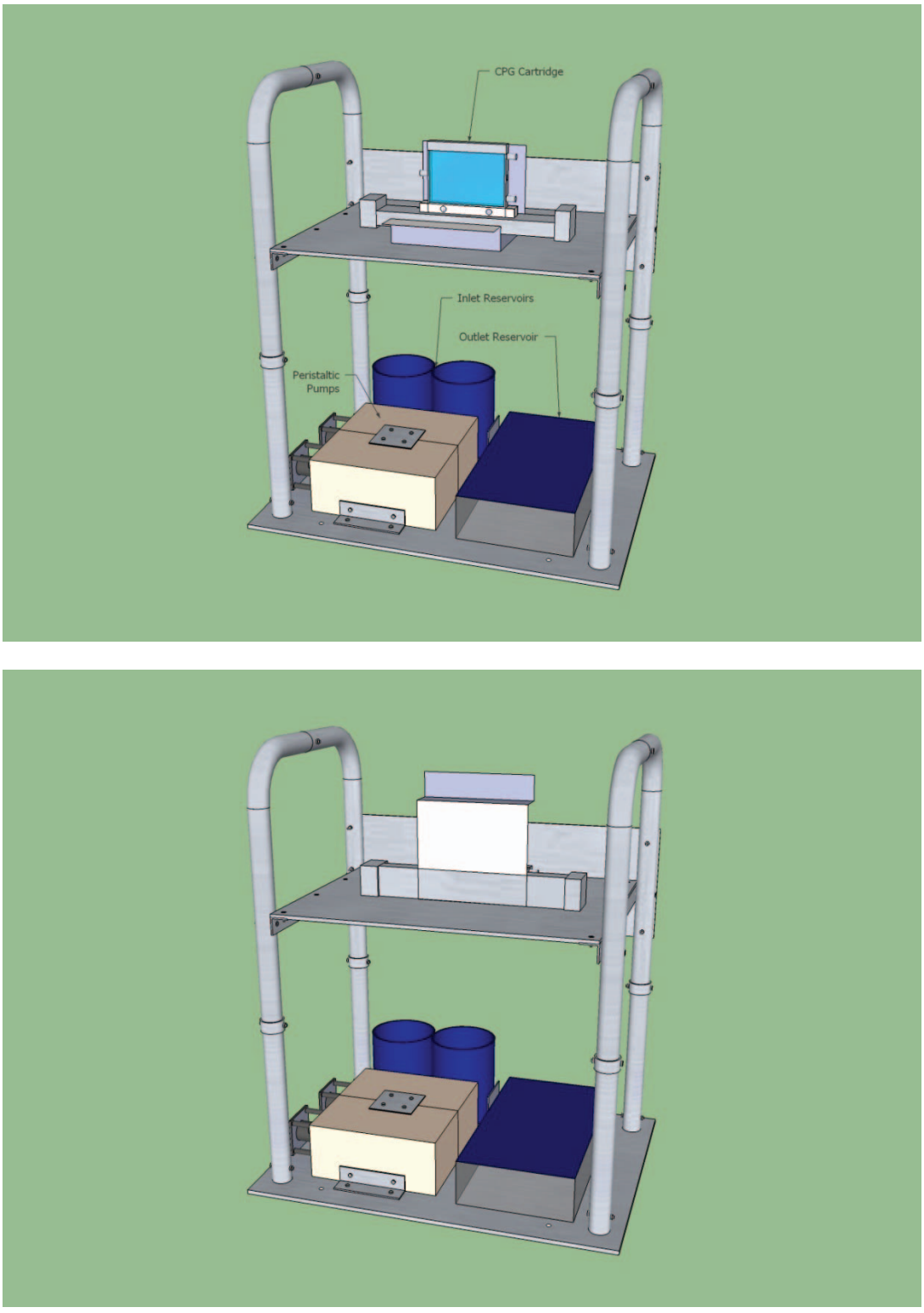

Figure 1.9. Prototype with CPG cartridge oriented Vertically (Top Schematic) or Horizontally (Bottom Schematic).

2.0 GROUND TESTING.

Ground tests were performed in a 1-g environment in our lab with CPG cartridges operated in both vertical and horizontal orientations. These ground tests were intended to exactly match the scheduled flight tests in both nature and number. Identical tests were performed using both the Teflon media and glass media CPG cartridges with the exception that the intermediate flow condition for the horizontal tests was omitted for the Teflon media cartridge due to the reduced number of zero-g parabolas available for the second day. For horizontal testing three flow ranges and gas liquid ratio combinations [water flow (cc/min), air flow (cc/min)] were used. The actual values were [43,12], [65,19] and [87,25]. During vertical testing for each cartridge was operated for a total of 6 minutes at the maximum combined fluid flow rates of 87 cc/min water and 25 cc/min air. Water and liquid volumes were not collected and recorded for the vertically oriented tests due to the practical limitations of fluid handling logistics and the nature of our planned zero-g experimental objectives (video comparison of gas-liquid separation spanning both reduced gravity and elevated gravity environments during each flight parabola). Explicitly, the extra collection bags/handling and required work-load of the zero-g fliers would have been excessive. Automated collection would have improved the situation somewhat, but experimental complexity and likelihood of in-flight failure would have remained high. Regardless video data for the vertical tests was of primary importance as seen from the results discussed below. Fluid volumes were instead collected during operation of the CPG cartridges in the horizontal orientation.

Figure 2.1 contains a photo linked to video of the operation of the glass media CPG cartridge while in the vertical orientation during ground testing. To view the video from the Word Document place cursor on photo and follow the screen tip instructions. To view the video from a PDF version place cursor on photo, left-click and open with Windows Media Player. An archive of these videos is also located within the Research section at the URC web link http://www.urc.cc/ under the CPG-GLS zero-g flight data page. The dynamic fluid distribution behavior between the upper and lower output ports for this video segment is representative of that observed during the entire 6 minutes of operation. Significant gas flow is observed at both the upper and lower outlet ports demonstrating relatively poor gas-liquid separation of the Glass media cartridge when

operating in 1-g. However, the fact that any portion of the gas flow occurs at the lower port does indicate that the CPG phenomena has some influence on the gas distribution

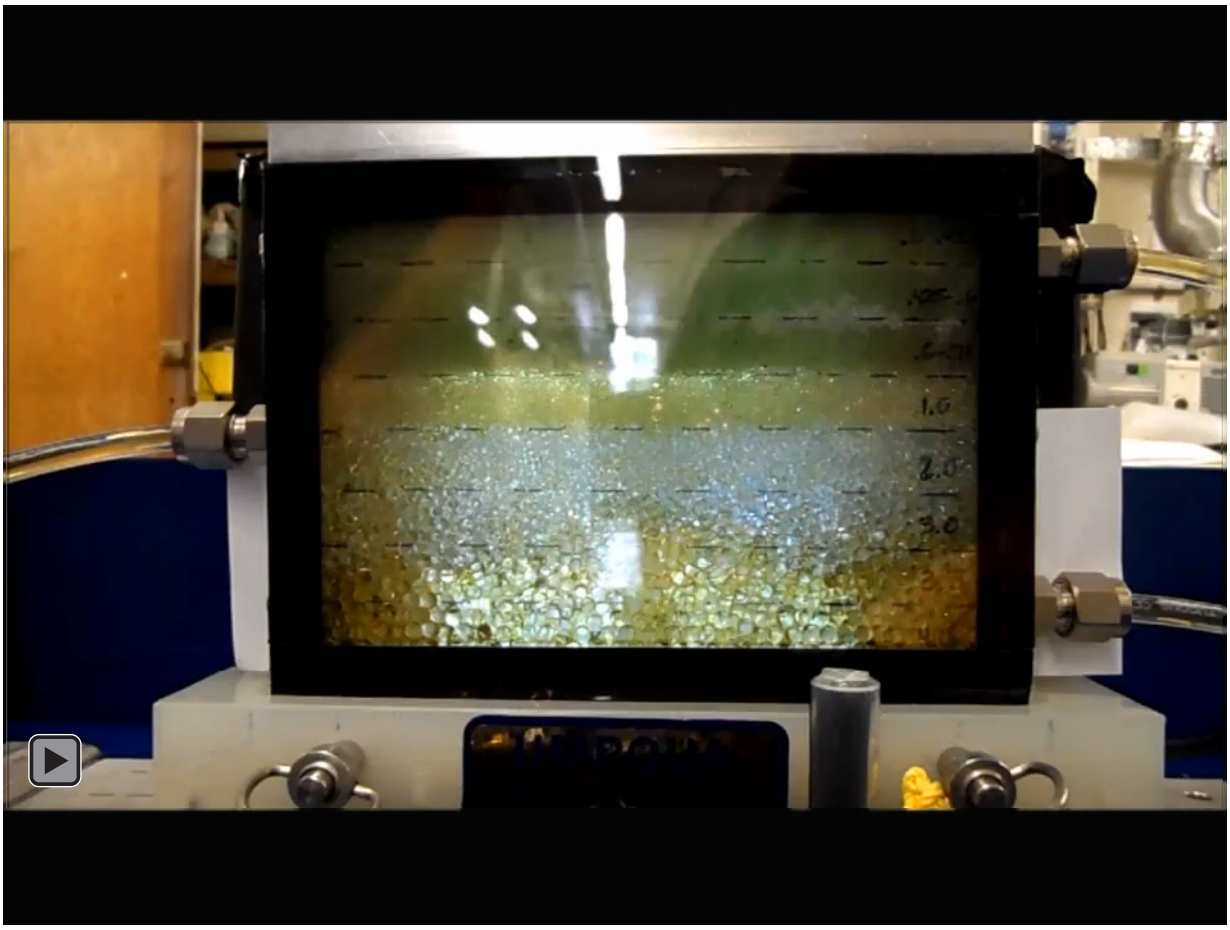

Figure 2.1. Glass media CPG cartridge vertically oriented during ground testing. (Click on image to play movie.)

given that we would expect (for either an empty bed or a uniformly sized and distributed granular media bed) that all the gas flow would normally exit through the top port due to familiar terrestrial buoyancy forces.

From the video collected during ground testing of the Teflon media CPG cartridge operated in the vertical orientation, gas bubbles were never observed to come out the top port (see photo in Figure 2.2 with linked video). The amount of liquid coming out the top port was not recorded due to the nature of our experimental flight plan as described above. Again, strictly video data was collected during vertical operation and only during horizontal operation were the cumulative fluid volumes collected at the outlet ports to quantify gas-liquid separation. From previous testing in our lab, however, the

bulk of the liquid flow was historically observed to come out the upper port for the Teflon media CPG cartridge due to both CPG forces and the fact that the coarser, and thus less flow restrictive media, is immediately adjacent this outlet port. Despite this lack of quantitative data for the vertical tests the fact that all the air was collected from the lower outlet port in opposition to the 1-g buoyancy force is nevertheless significant.

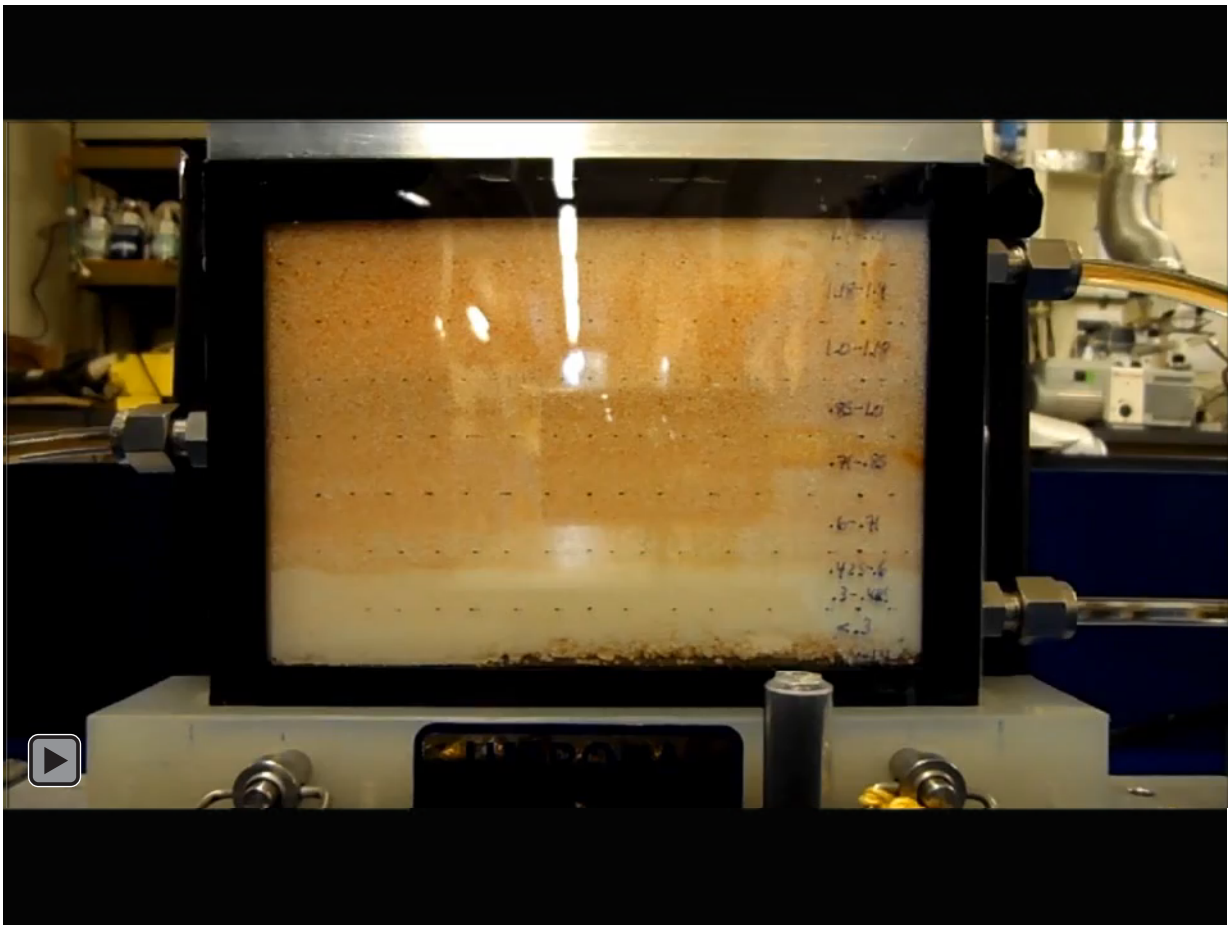

Figure 2.2. Teflon media CPG cartridge vertically oriented during ground testing. (Click on image to play movie.)

Quantitative gas-liquid separation testing was subsequently carried out with each CPG cartridge placed in a horizontal orientation as shown in Figure 2.3. In this orientation a CPG cartridge only experiences gravity/buoyancy forces acting perpendicular to the capillary pressure gradient forces rather than in direct linear opposition as when the cartridge is vertically oriented. As such, given that only an insignificant influence on separation performance arises from any buoyancy induced gas accumulation (collecting beneath the upper glass plate) for a horizontal cartridge,

capillary pressure gradient driven gas-liquid separation phenomena can be observed. In fact, CPG cartridge operation in the horizontal orientation should approximate operation in zero-g.

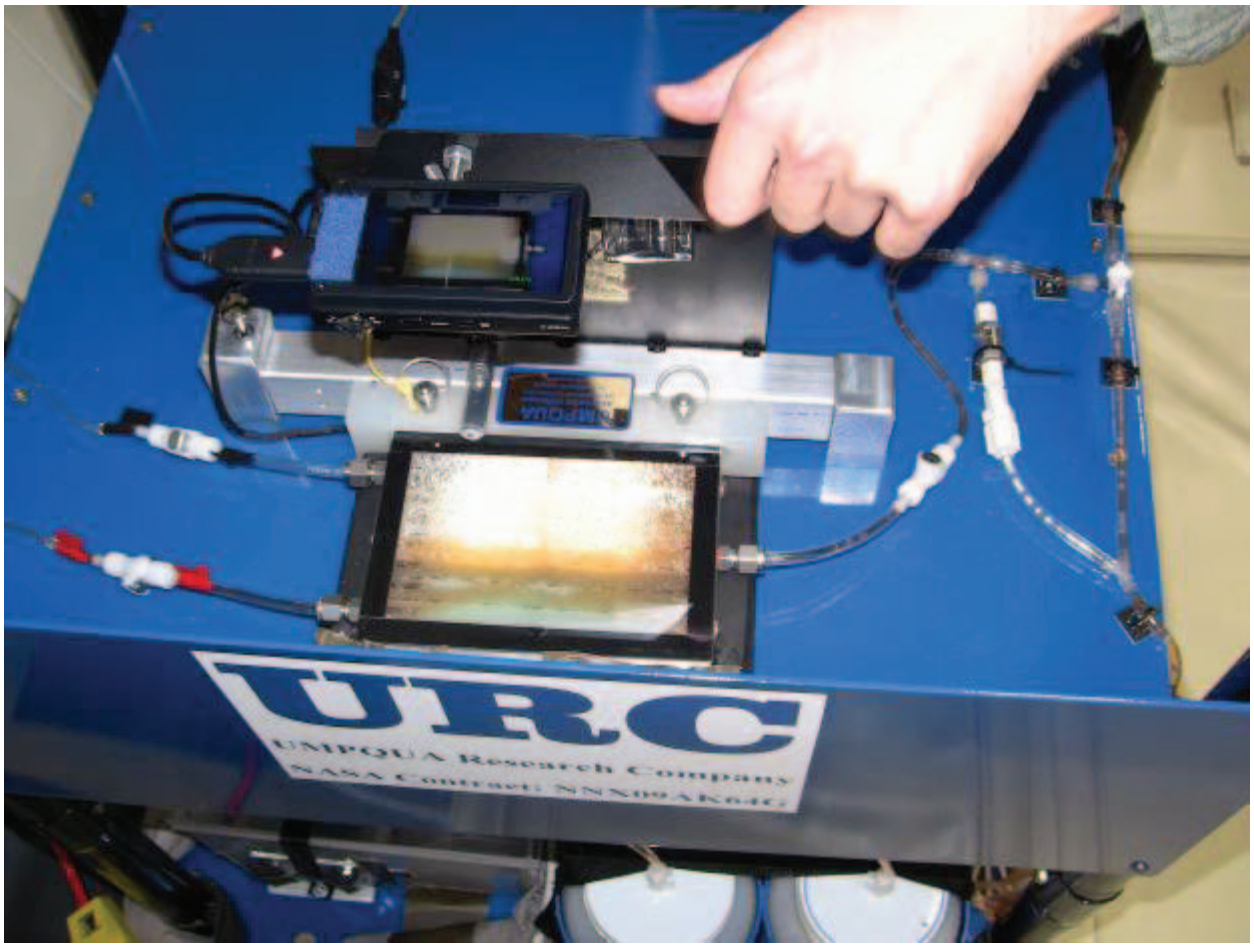

Figure 2.3. Glass media CPG cartridge oriented horizontally for quantitative gas-liquid separation testing.

Data collected during ground testing of the CPG cartridges in the horizontal orientation is summarized in the plots contained in Figures 2.4 and 2.5. Significant separation of the gas and liquid components to the “lower” and “upper” ports, respectively, is clearly demonstrated over a range of flow rates for both the glass media and Teflon media CPG cartridges. While not accomplishing complete separation of either phase at any of the influent flow rates, the bulk of the water is collected at the upper port and the bulk of the air is collected at the lower port.

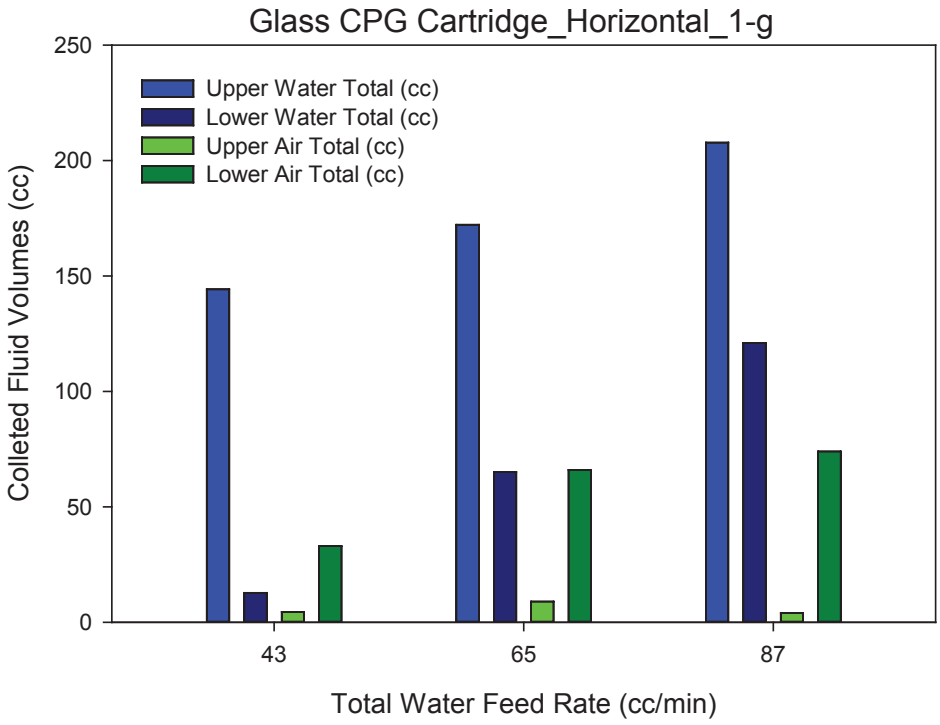

Figure 2.4. Glass media CPG cartridge Air-Water separation results for horizontal ground testing.

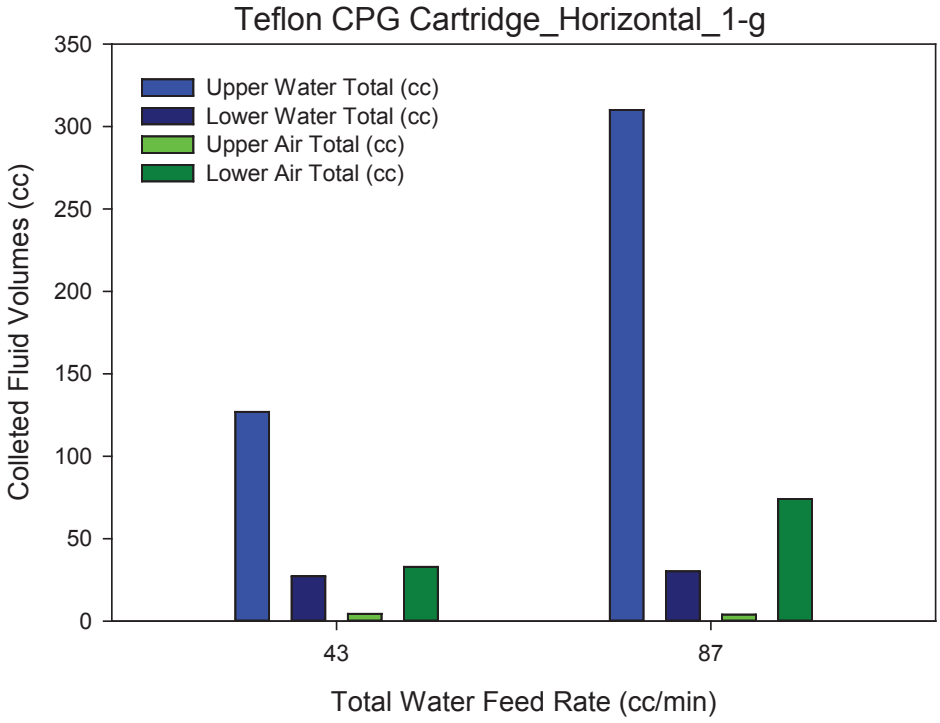

Figure 2.5. Teflon media CPG cartridge Air-Water separation results for horizontal ground testing.

3.0 FLIGHT TESTING.

Two Umpqua Research employees, John Holtsider and Dalton Deeks, served as our flight crew (fliers) on NASA's reduced gravity flight. Final preparation and evaluation of the GLS were performed on-site, April 30, 2012, at NASA-JSC's Ellington Field as shown in the photos seen in Figure 3.1. Minor modifications were made to the test rig addressing reviewer comments following the pre-flight Test Readiness Review. Actual flight dates for the CPG-GLS experiments were May 1st and 2nd , 2012..

Figure 3.1. Preparation of CPG-GLS prototype for Test Readiness Review and flight.

Figure 3.2 shows photos of the prototype and fliers just prior to and during the zero-g test conditions. Water colored with food dye was prepared prior to flight to serve as the feed liquid during flight testing. Predetermined air/water mixtures at various total flow rates were introduced to the CPG cartridge under test via a pair of peristaltic pumps. Cumulative air/water mixtures were collected (for post flight analysis) in

separate collapsible bags from each horizontal CPG cartridge's upper and lower outlet ports.

Figure 3.2. Pre-parabola preparation (top photos) and operation during zero-g testing (lower photos).

Since we were allotted two flight days in which to perform our reduced gravity testing and we had two CPG cartridges we decided to assign one CPG cartridge for each day. The Glass media CPG cartridge was evaluated on the first flight day and the Teflon media CPG cartridge on the second day. The original experimental flight schedule for CPG-GLS testing is shown in Table 3.1. Horizontal testing was planned at the beginning of each day with flow rates gradually increased. Vertical testing, scheduled for the end of each day, was to be performed at the highest flow rate setting thereby allowing rapid equilibration (for good video data) of phase distribution between the outlet ports during the brief 20 second zero-g interval of each parabola.

Table 3.1. CPG-GLS Experimental Flight Plan Schedule.

Parabola Series	Parabola	Day 1 Glass Media	Day 2 Teflon Media
		Cell orientation (VT=Vertical with water collected at Top, or H=Horizontal). Flow conditions (Water and Air Flow Rates, respectively, in mL/min)	
1	1	*H,43,12 (bypass flow in 2g)	*H,43,12 (bypass flow in 2g)
	2	H,43,12	H,43,12
	3	H,43,12	H,43,12
	4	H,43,12	H,43,12
	5	H,43,12	H,43,12
	6	H,43,12	H,43,12
	7	H,43,12	H,43,12
	8	H,43,12	H,43,12
	9	H,43,12	H,43,12
	10	H,43,12	H,43,12
5-10 min. break		Swap Bags & Raise Flows	Swap Bags & Raise Flows
2	11	H,65,19 (bypass flow in 2g)	H,87,25 (bypass flow in 2g)
	12	H,65,19	H,87,25
	13	H,65,19	H,87,25
	14	H,65,19	H,87,25
	15	H,65,19	H,87,25
	16	H,65,19	H,87,25
	17	H,65,19	H,87,25
	18	H,65,19	H,87,25
	19	H,65,19	H,87,25
	20	H,65,19	H,87,25
5-10 min. break		Swap Bags & Raise Flows	Swap Bags & Cell Vertical
3	21	H,87,25 (bypass flow in 2g)	VT,87,25 (pump continuous)
	22	H,87,25	VT,87,25
	23	H,87,25	VT,87,25
	24	H,87,25	VT,87,25
	25	H,87,25	VT,87,25
	26	H,87,25	VT,87,25
	27	H,87,25	VT,87,25
	28	H,87,25	VT,87,25
	29	H,87,25	VT,87,25
	30	H,87,25	VT,87,25
5-10 min. break		Swap Bags & Cell Vertical	Swap Bags for Lunar gravity
4	31	VT,87,25 (pump continuous)	VT,87,25 (pump continuous)
	32	VT,87,25	VT,87,25
	33	VT,87,25	VT,87,25
	34	VT,87,25	VT,87,25
	35	VT,87,25	VT,87,25
Break- day 2 only			Swap Bags for Mars gravity
	36	VT,87,25	VT,87,25 (pump continuous)
	37	VT,87,25	VT,87,25
	38	VT,87,25	VT,87,25
	39	VT,87,25	VT,87,25
	40	VT,87,25	VT,87,25

Testing under the Mars and Lunar gravity conditions was originally scheduled for the end of the second day using the Teflon CPG cartridge operated in the vertical orientation. Due to early termination of the first day's flight tests, video of the Glass media cartridge in the vertical orientation was not collected. In order to not lose the vertical video data for the Teflon CPG cartridge as well, the test plan for the second day was altered such that the vertical test was to be performed first. Fortunately both the Martian and Lunar gravity test conditions, which were planned for our vertical testing, had also been reassigned to the first part of the second day's flight and all the vertical tests could still be executed sequentially as originally intended.

A photo with linked video obtained during preliminary loading of the Teflon media cell just prior to the first Martian parabola on day 2 is contained in Figure 3.3. Similarly,

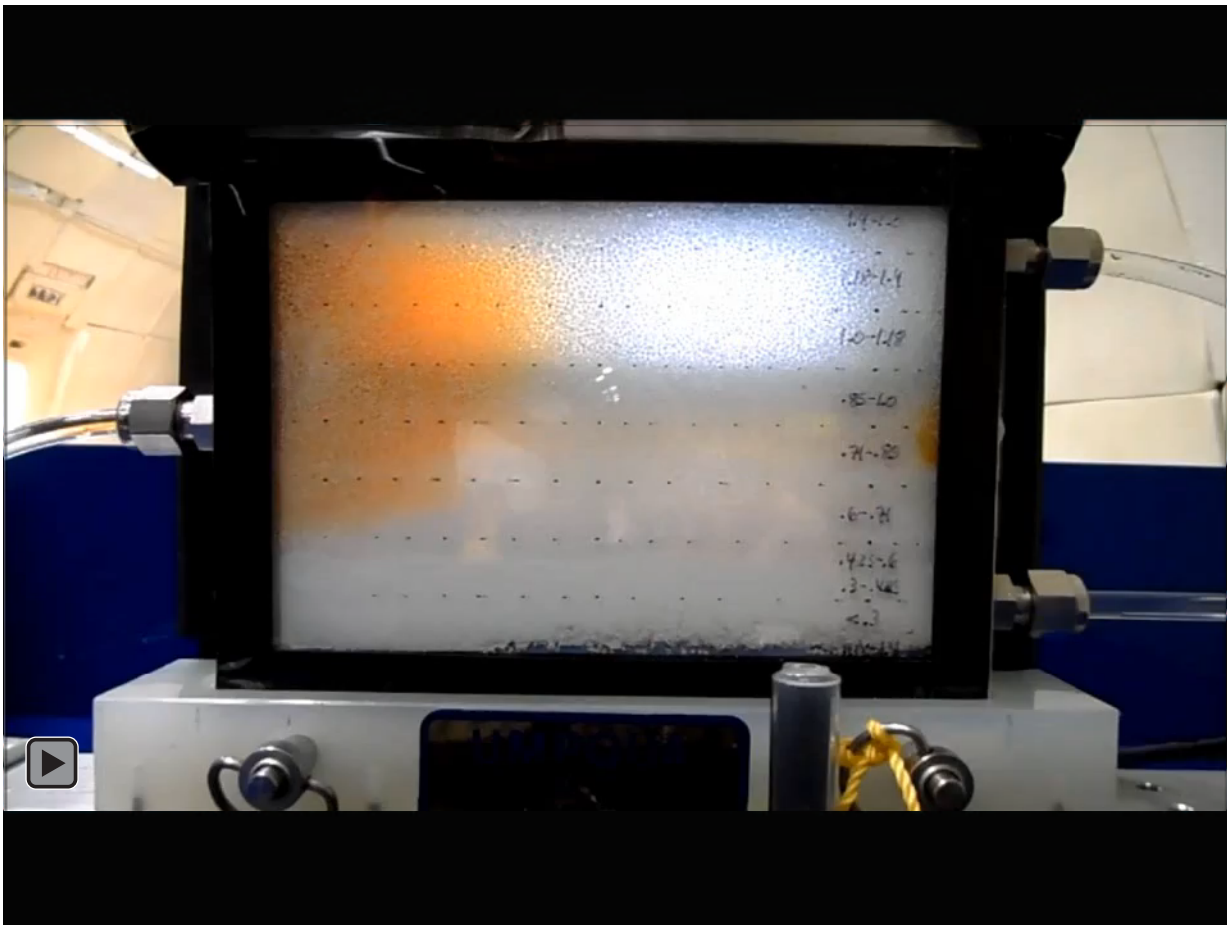

Figure 3.3. Teflon media CPG cartridge vertically oriented in flight during pre-parabola 1-g equilibration with air/colored water mixture displacing water from an initially pure water filled cartridge. (Click on image to play movie.)

representative operation during each of the reduced gravity conditions, Martian-g, Lunar-g and zero-g, is shown in the photos (each with linked video) contained in Figures 3.4, 3.5 and 3.6, respectively. Recording time for each of the reduced gravity videos spans the time in the elevated gravity state (1g+) just prior to the reduced gravity condition proceeding through the complete reduced gravity state until the elevated (1g+) gravity is re-established. Each of these videos shows a clear change in the gas liquid separation state of the Teflon cartridge as it transitions from elevated gravity to reduced gravity and then back again to elevated gravity. In the elevated gravity state there is clearly little, if any, difference in gas distribution between the upper and lower ports. However, as soon as the system is exposed to reduced gravity, all the gas flow switches to the lower port and remains there until elevated gravity is retained.

These videos clearly demonstrate that effective 100% gas separation from the liquid stream is feasible using the CPG-GLS technology under a wide range of gravity environments ranging from Martian gravity to Lunar gravity to zero-g. In fact, a balance of forces must exist somewhere between the elevated gravity (1g+) and the 1/3-g Martian states, which implies effective operation at local gravities (i.e., larger planetary bodies) in excess of those found on Mars. In addition, it is noteworthy that this Teflon CPG cartridge, while arguably a stronger separator than the Glass media cartridge (since Teflon is more hydrophilic in magnitude, than glass is hydrophobic in magnitude) is clearly far from optimal in its design. Formed from 8 coarse layers of granular Teflon media of monotonically increasing size, this cartridge was designed (due to practical limitations related to material availability and processing) to merely demonstrate the CPG-GLS effect and clearly leaves much room for improvement.

While not acquiring video for the glass media bed as intended, it is expected that similar separation phenomena would have been observed, albeit with the balance of gravitational and CPG forces occurring at a lower effective gravity than for the Teflon media cartridge (e.g., 0.6g for glass media cartridge vs. 0.9g for Teflon media cartridge), again due to the difference in relative magnitudes of the corresponding hydrophobic and hydrophilic surface forces.

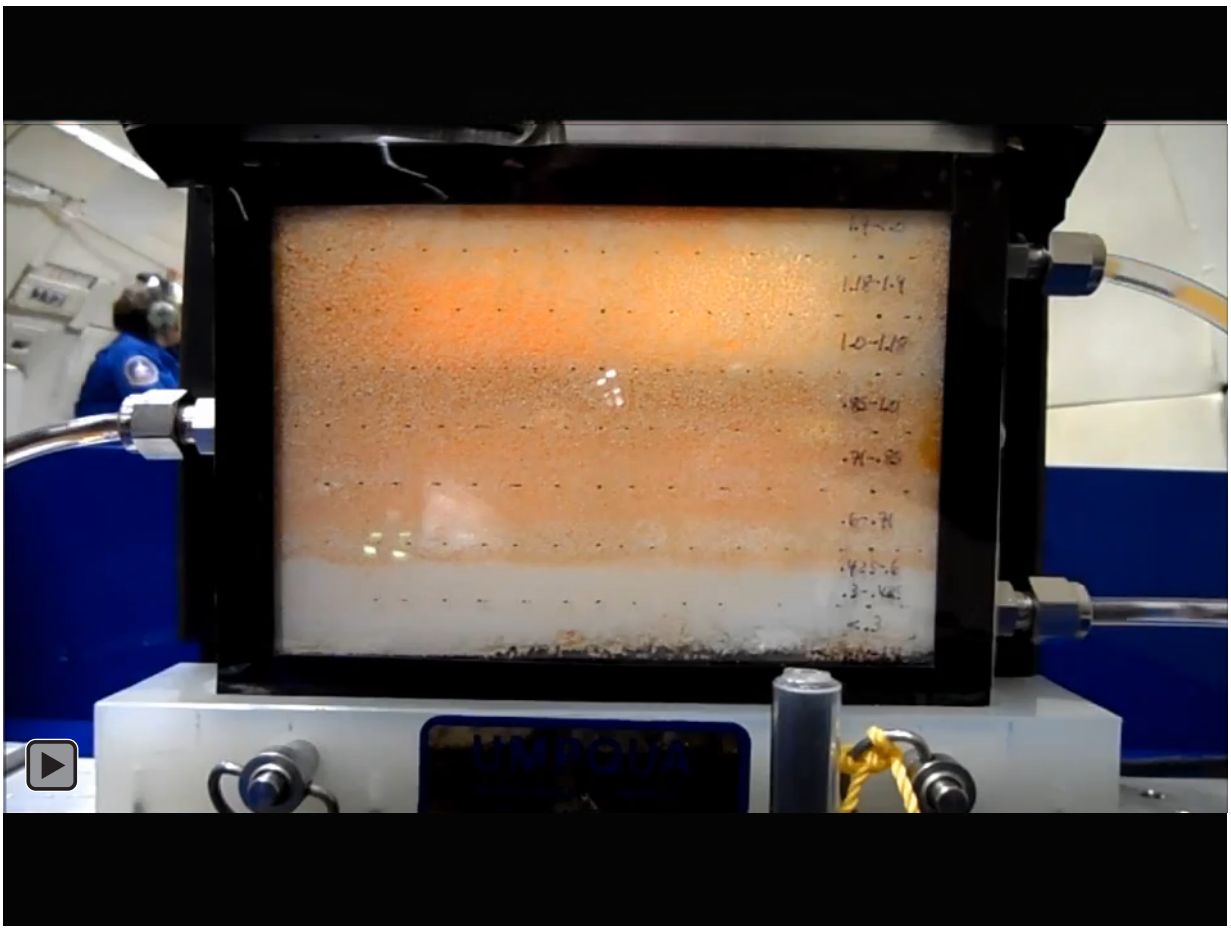

Figure 3.4. Teflon media CPG cartridge vertically oriented in Mars-gravity. (Click on image to play movie.)

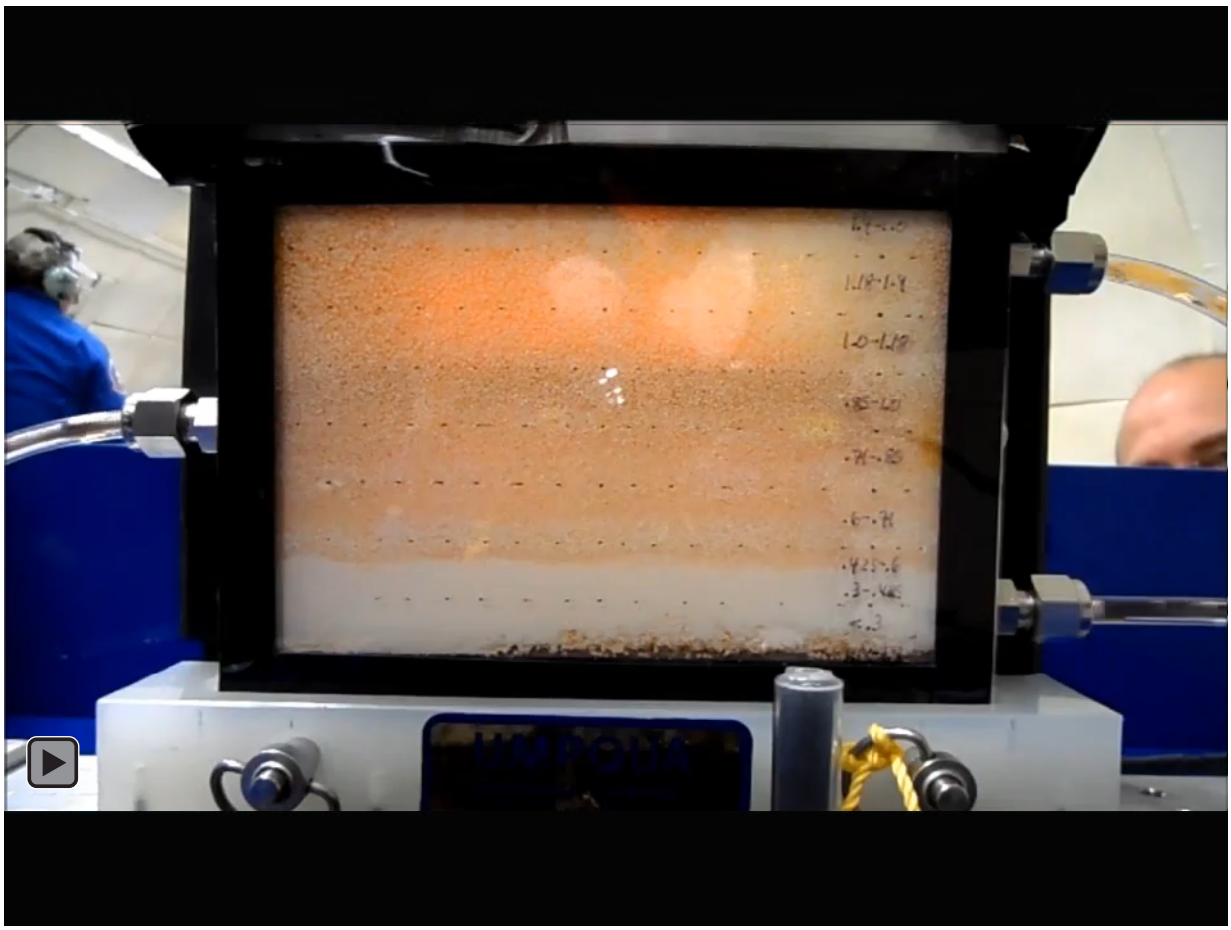

Figure 3.5. Teflon media CPG cartridge vertically oriented in Lunar-gravity. (Click on image to play movie.)

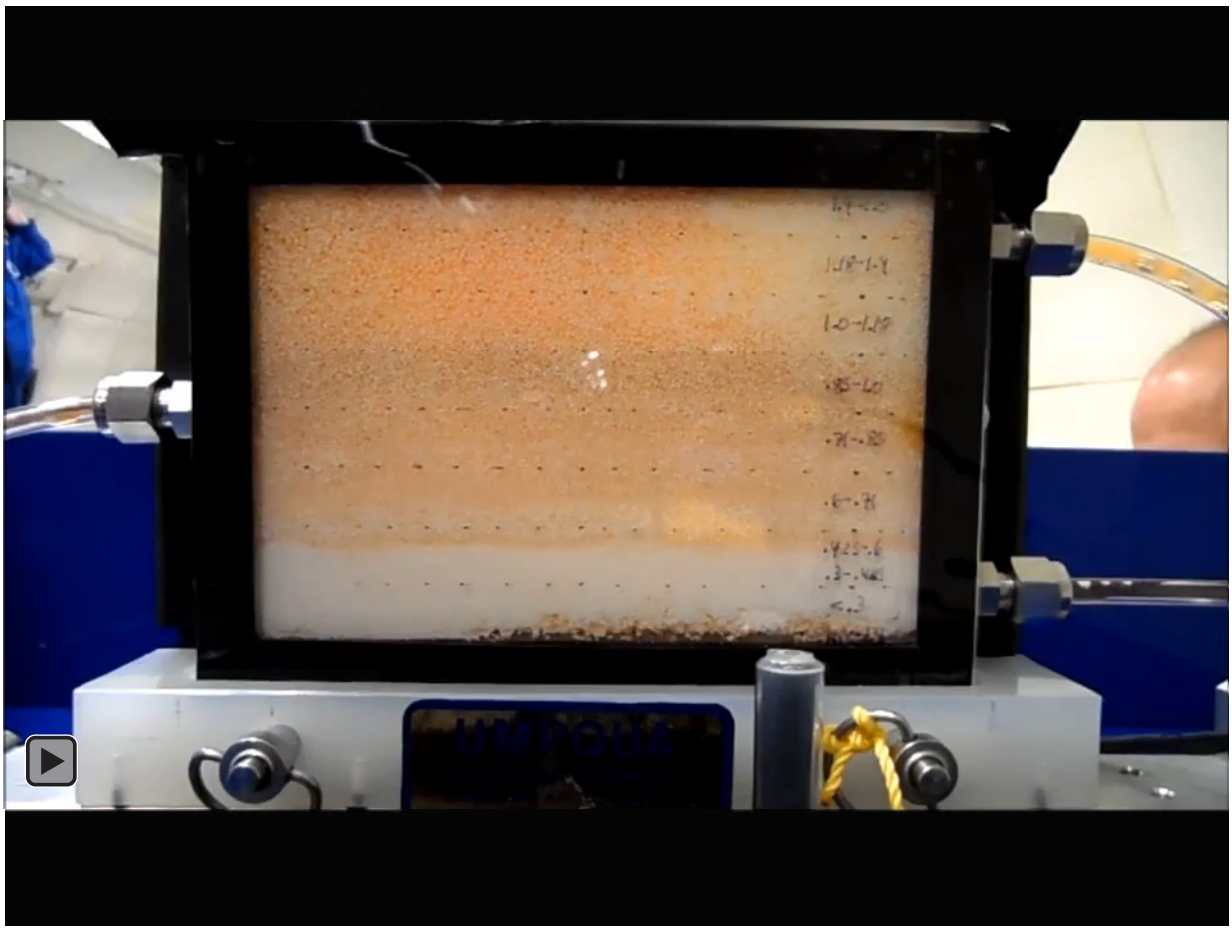

Figure 3.6. Teflon media CPG cartridge vertically oriented in zero-g. (Click on image to play movie.)

Flight data collected during operation of the CPG cartridges in the horizontal orientation are summarized in the plots contained in Figures 3.7 and 3.8. Again, identical tests were performed for both the Teflon media and glass media CPG cartridges with the exception that the intermediate flow condition was omitted during horizontal operation with Teflon. For horizontal flight testing, three flow ranges and gas liquid ratio combinations [water flow (cc/min), air flow (cc/min)] were used. These included [44,11], [71,19] and [93,26]. During the vertical testing, described above, the cartridges were operated for the duration of each parabola series (Mars-g, Lunar-g, and zero-g) at the maximum combined fluid flow rates of [93,26]. As with the corresponding results from ground (1-g) testing in the horizontal orientation, as shown in Figures 2.4 and 2.5, significant separation of the gas and liquid components is observed between the lower and upper outlet ports, respectively. The gas separation data at the lower

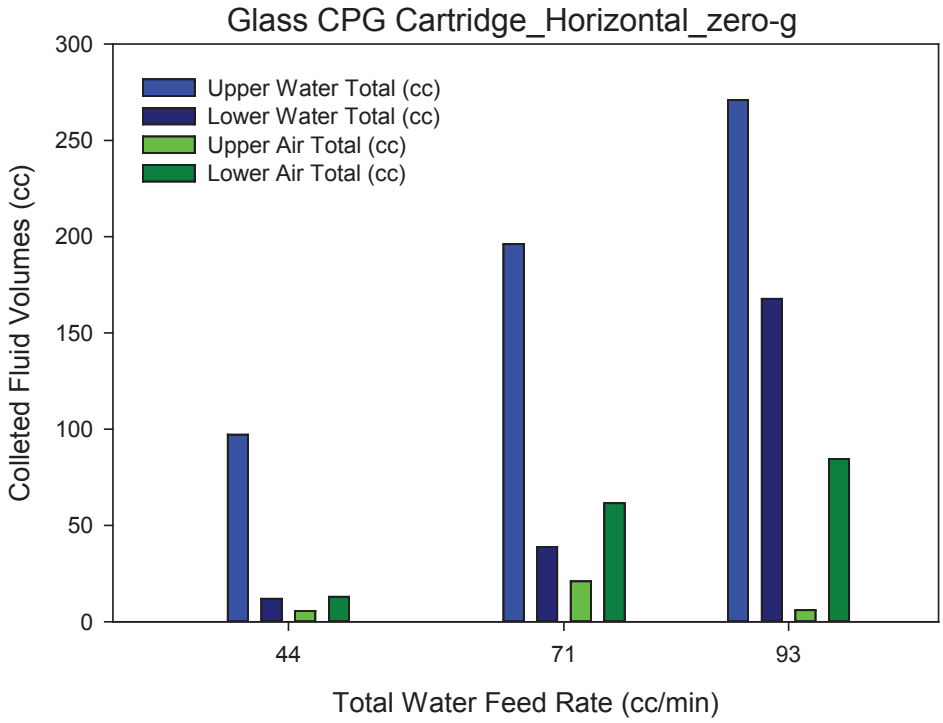

Figure 3.7. Glass media CPG cartridge Air-Water separation results for horizontal zero-g testing.

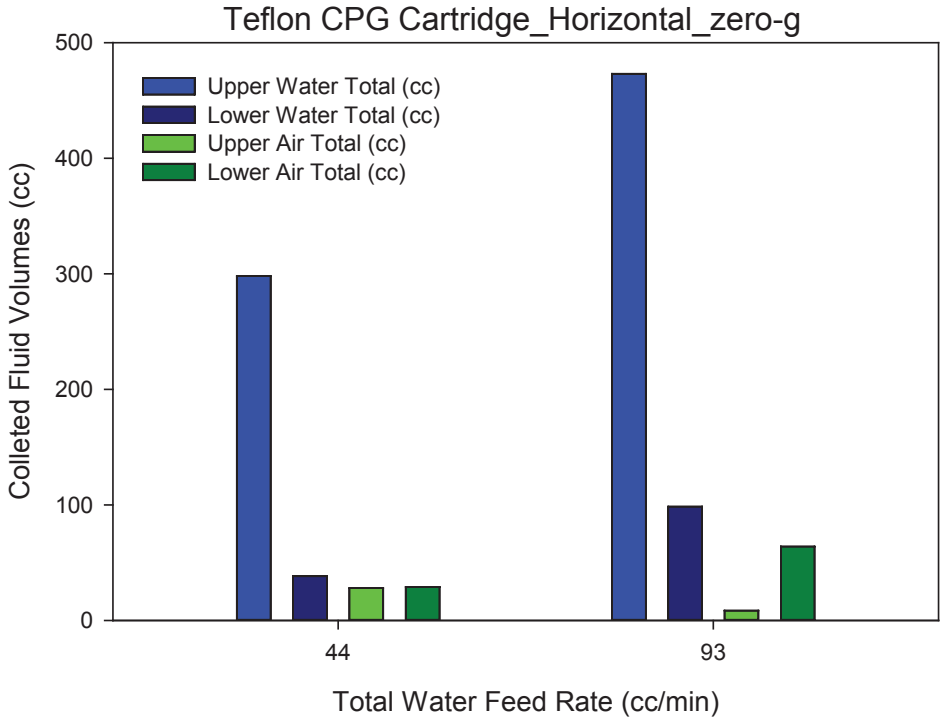

Figure 3.8. Teflon media CPG cartridge Air-Water separation results for horizontal zero-g testing.

flow rate, alone, is observed to be somewhat poorer for zero-g testing compared to ground tests. Due to the relatively low volumes collected this difference could easily be due to experimental error. Most importantly, however, due to the generally good agreement between the zero-g and ground separation test results it appears that our assumption that operation of the CPG cartridges in the horizontal orientation while in a 1-g environment does indeed reasonably approximate separation functionality of the same cartridges operating in a zero-g environment. Therefore horizontal operation of a CPG-GLS cartridge in 1-g is a good zero-g analog.

4.0 Modeling Pin-Plate Separator with Lattice Boltzmann Method

In this work, simulations were setup to study the pin plate separator using the previously developed lattice Boltzmann model. The purpose of this work was exploratory – to make an initial study of the pin plate gradients and to determine the effect that the different design and operating parameters may have on the performance of a pin plate separator device. Information on the pin plate geometries, the fluid model and boundary conditions and simulation results are presented below. As mentioned in the previous report (Second year report - Grant Number: NNX09AK64G) a commitment was made to design, manufacture and build a pin-plate separator if numerical simulations would have yielded positive results. Assessment of Lattice-Boltzmann modeling results indicated that an experimental effort should be made to verify the feasibility of phase separations in a pin-plate separator. One should notice that the nature of this numerical and experimental development represents only a *feasibility study* work effort. The approach taken in this feasibility study was conceived during the second year of the project (thus, it was not proposed in the original proposal) as a result of discoveries made in the experimental part of the originally proposed project.

4.1 Thin plate correction

The lattice Boltzmann simulations were setup in two dimensions. To account for the viscous forces resulting from the presence of walls in the un-modeled third dimension, a thin plate correction was used as an additional force in the model. The approach taken in this derivation is definitively an original development for applications in fluidic simulation in microscale-based structures. *Thin-plate-correction* effectively turns a 2D simulation into a quasi -3D simulation with well-controlled and known error. The derivation and results of this thin plate correction are presented below.

A two-dimensional model typically assumes that the distances in the third unrepresented dimension are large enough that there won't be an effect on the flow in the model. For the case of the pin plate separator, however, the gap between the plates is very thin, ~250 μm or so, and traditional assumptions are no longer valid. To model the thin space between the plates, a correction term is added to the 2D model.

In the x-direction, the correction term is obtained by starting with the x-direction component of the Navier-Stokes equations.

$$\rho\left(\frac{\partial \boldsymbol{u}_x}{\partial \boldsymbol{t}}+\boldsymbol{u}_x\frac{\partial \boldsymbol{u}_x}{\partial \boldsymbol{x}}+\boldsymbol{u}_y\frac{\partial \boldsymbol{u}_x}{\partial \boldsymbol{y}}+\boldsymbol{u}_z\frac{\partial \boldsymbol{u}_x}{\partial \boldsymbol{z}}\right)=-\frac{\partial \boldsymbol{p}}{\partial \boldsymbol{x}}+\mu\left(\frac{\partial^2 \boldsymbol{u}_x}{\partial \boldsymbol{x}^2}+\frac{\partial^2 \boldsymbol{u}_x}{\partial \boldsymbol{y}^2}+\frac{\partial^2 \boldsymbol{u}_x}{\partial \boldsymbol{z}^2}\right)+\rho \boldsymbol{g}_x \qquad \text{Eq-4.1}$$

Examining the terms with a *z*-direction dependence, it is still appropriate to assume that $\boldsymbol{u}_z = 0$ for the pin plate separator. This leaves $\mu\frac{\partial^2 \boldsymbol{u}_x}{\partial \boldsymbol{z}^2}$ as the only term requiring consideration.

To develop a correction term, it is assumed that the flow is laminar and has a parabolic profile in the z-direction. For flow between two plates with spacing *H* apart, the well-known equation for this profile is given as:

$$\boldsymbol{u}_x(\boldsymbol{z})=6\overline{\boldsymbol{u}}_x\frac{\boldsymbol{z}}{\boldsymbol{H}}\left(1-\frac{\boldsymbol{z}}{\boldsymbol{H}}\right) \qquad \text{Eq-4.2}$$

where $\overline{\boldsymbol{u}}_x$ is the x-direction velocity averaged over the entire *z*-dimension. In a 2D model, the *z*-average of the *x*-direction velocity is being solved, so $\boldsymbol{u}_{x,2D}=\overline{\boldsymbol{u}}_x$. Evaluating the $\mu\frac{\partial^2 \boldsymbol{u}_x}{\partial \boldsymbol{z}^2}$ for this profile,

$$\mu\frac{\partial^2 \boldsymbol{u}_x}{\partial \boldsymbol{z}^2}=-\mu\frac{12}{\boldsymbol{H}^2}\overline{\boldsymbol{u}}_x \qquad \text{Eq-4.3}$$

Averaged over the z-dimension:

$$\left.\mu\frac{\partial^2 \boldsymbol{u}_x}{\partial \boldsymbol{z}^2}\right|_{avg}=-\frac{1}{\boldsymbol{H}}\int_0^{\boldsymbol{H}}\mu\frac{12}{\boldsymbol{H}^2}\overline{\boldsymbol{u}}_x d\boldsymbol{z}=-\mu\frac{12}{\boldsymbol{H}^2}\overline{\boldsymbol{u}}_x \qquad \text{Eq-4.4}$$

This correction term can show up as a force term in the 2D Navier-Stokes equations.

$$\rho\left(\frac{\partial \boldsymbol{u}_x}{\partial \boldsymbol{t}}+\boldsymbol{u}_x\frac{\partial \boldsymbol{u}_x}{\partial \boldsymbol{x}}+\boldsymbol{u}_y\frac{\partial \boldsymbol{u}_x}{\partial \boldsymbol{y}}\right)=-\frac{\partial \boldsymbol{p}}{\partial \boldsymbol{x}}+\mu\left(\frac{\partial^2 \boldsymbol{u}_x}{\partial \boldsymbol{x}^2}+\frac{\partial^2 \boldsymbol{u}_x}{\partial \boldsymbol{y}^2}\right)+\rho \boldsymbol{g}_x-\mu\frac{12}{\boldsymbol{H}^2}\boldsymbol{u}_x \quad \text{Eq-4.5}$$

A similar development can be followed to create a correction term for the y-direction Navier-Stokes equations.

$$\rho\left(\frac{\partial \boldsymbol{u}_y}{\partial \boldsymbol{t}}+\boldsymbol{u}_x\frac{\partial \boldsymbol{u}_y}{\partial \boldsymbol{x}}+\boldsymbol{u}_y\frac{\partial \boldsymbol{u}_y}{\partial \boldsymbol{y}}\right)=-\frac{\partial \boldsymbol{p}}{\partial \boldsymbol{y}}+\mu\left(\frac{\partial^2 \boldsymbol{u}_y}{\partial \boldsymbol{x}^2}+\frac{\partial^2 \boldsymbol{u}_y}{\partial \boldsymbol{y}^2}\right)+\rho \boldsymbol{g}_y-\mu\frac{12}{\boldsymbol{H}^2}\boldsymbol{u}_y \quad \text{Eq-4.6}$$

To test the correction factor, 3D channel flow of air and water was simulated using the 2D model with thin-plate correction. For flow in a square channel, the relationship between pressure drop ($\Delta \boldsymbol{P}$), flow rate (*Q*), viscosity (μ), channel height and width (*a* and *b*), and channel length (*L*) is given as:

$$\boldsymbol{Q}=\frac{\boldsymbol{a}\boldsymbol{b}^3\Delta \boldsymbol{P}}{\boldsymbol{K}\mu \boldsymbol{L}} \quad \text{Eq-4.7}$$

where ***K*** is dependent on the ratio of ***a/b***:

***a / b*=**	1	1.5	2	3	4	5	10	∞
***K* =**	28.45	20.43	17.49	15.19	14.24	13.73	12.81	12

Results of this test are shown in Table 4.1. Examination of the results shows that the correction does better at higher aspect ratios (where the correction term dominates) than when the channel width and height are close to the same dimension. Even so, at 10 to 15% the error is likely acceptable for a 2D model. It should be noted that the error is also a function of viscosity parameters in the lattice Boltzmann method, which is the source of the differences between the flow rate error between air and water cases.

Table 4.1 - Thin plate correction error.

Fluid	Channel Width	Channel Height	Aspect Ratio	Flow rate % Error
Air	275 μm	250 μm	1.1	11.75%
Water	275 μm	250 μm	1.1	15.58%
Air	975 μm	250 μm	3.9	2.52%
Water	975 μm	250 μm	3.9	1.91%

4.2 Pin Plate Separator Models

The objective of this effort was to use the CFD model to numerically explore the various parameters that require consideration when designing a pin plate separator. These parameters represent the most important enabling properties of the pin-plate on which the functionality and performance of the plate greatly depends. The parameters explored in this feasibility study are:

Gas/Liquid Flow Rate – The total flow rate of a gas/liquid mix that can be processed by a device directly determines the relationship between the size, weight, and cost of a device for a stated capacity. Since pin-plate devices are “numbered” up, rather than scaled-up, there is a direct relationship between device capacity and the size, volume and weight of a device. Numbering-up approach allows the introduction of sufficient number of parallel plates to effectively mediate average velocity of fluids flowing through the plate.

Contact Angle – Solid surfaces in a pin plate separator can have a hydrophobic or hydrophilic nature to them – either due to a surface treatment or due to the intrinsic solid material properties used for the construction of the pin plate. The use of a surface treatment to create a hydrophilic or hydrophobic treatment may require additional maintenance during long-term device usage and it is less preferred. Practical experience shows that processing fluids that contain even small amounts of dissolved proteins typically require appropriate coating of surfaces of microscale-based structures.

Thus, appropriate design will take into account the need to periodically renew the surface coating in this kind of devices.

Air/Water Mix – The air/water mix is the ratio of air to water in a mixed-phase stream to be processed by the pin-plate separator. In an ideal case, a device would operate independently of the air/water mix being fed into it and a device would be able to separate a small amount of water from an air stream as efficiently as it could separate a small amount of air from a water stream. Understanding the separation effectiveness of a pin-plate separator at different air/water ratios will allow the pin-plate separator to be used in situations where it will be most effective at separating air/water mixtures.

Pin Diameter Gradient – The pin diameter gradient is the rate at which the diameters of the pins change along cardinal space directions. A higher pin gradient should exhibit a stronger separation but will in many cases be more challenging to fabricate.

Outlet Conditions – The total flow rate leaving a device at the device outlets can strongly affect the gas/liquid separation happening within the device. In a microdevice, outlet flow rates can be difficult to control due to typically very low pressure-drop through the device. Installing back-pressure valves at the exit stream lines typically mediates this challenge.

4.3 Simulation Geometries

Two small separator geometries were set up to simulate the air-water separation in the pin-plate separation design. The geometries, shown in *Figure 4.1* and *Figure 4.2*, are designed to be large enough to observe and measure gas-liquid separation effects yet small enough to allow a series of simulations to be performed in a reasonable amount of time.

Both geometries consist of an inlet, two outlets, and a five by seven array of staggered pins inside a domain that is 3200 microns long and 1600 microns wide. The distance between the plates, used in the thin-plate correction, is assumed to be 250 microns.

In the first pin plate separator, labeled pin plate separator geometry #1, the pins range from 225 microns to 325 microns in diameter with a pin diameter gradient of 25 microns per 400 microns. In the second pin plate separator, labeled Pin Plate

Separator Geometry #2, the pins range from 150 microns to 350 microns in diameter with a pin diameter gradient of 50 microns per 400 microns.

Note that the local pin-diameter gradient in this simulation is rather high and cannot be easily manufactured using standard micromachining in polymers and metals. It is also important to note that the definition of the characteristic size of the *locality* (local space) is defined by the average size of the bubble (discrete phase). In the pin=plate experimental effort, (see Section 5) the overall size of the plate was much larger (18x12 cm) thus local pin-diameter gradient necessarily had to be smaller. This has large repercussions on the smallest size of the bubble that can be effectively processed through pin-plate separator.

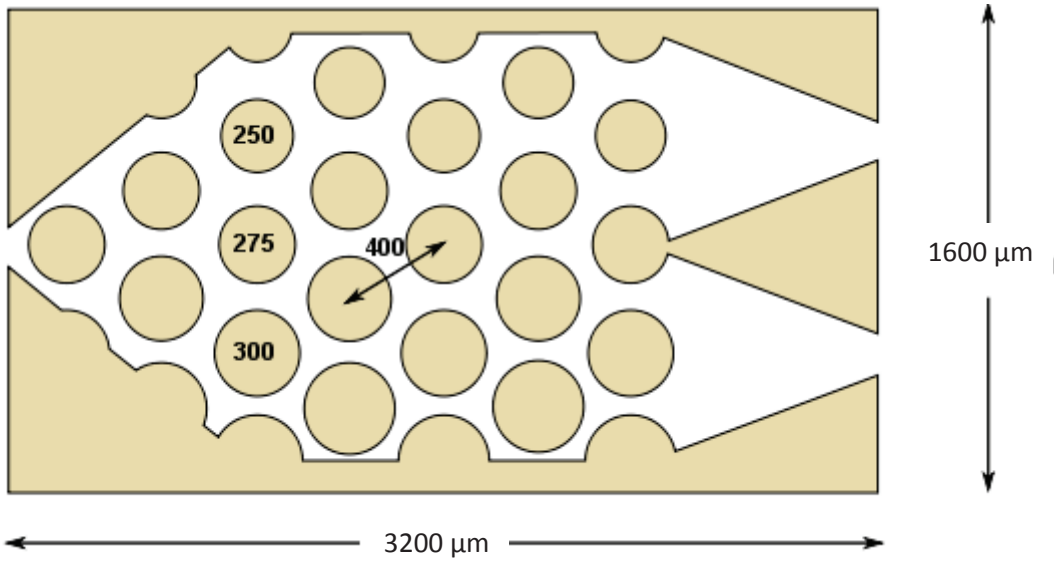

Figure 4.1. Pin plate separator geometry #1.

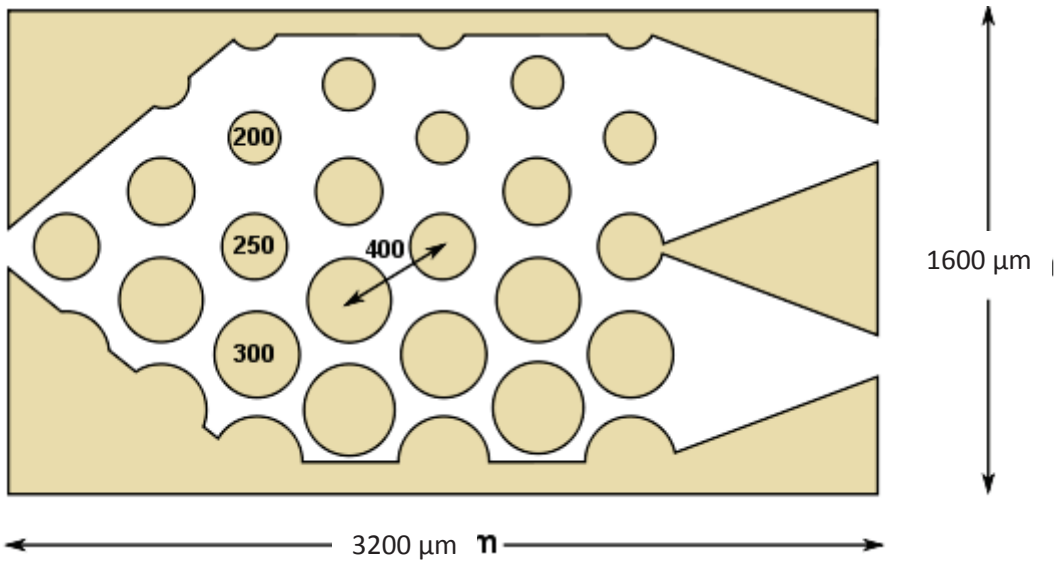

Figure 4.2. Pin plate separator geometry #2.

4.4.1 Boundary Conditions

The boundaries of the geometry are labeled the inlet, upper outlet, and lower outlet as shown in *Figure 4.3*. In the simulations performed the inlet flow rate was varied from 1.0 to 3.0 µL/s and was composed of 25% to 75% air in water. Regardless of the flow rate or air water mix, the air bubble size was 0.05 µL.

In most simulations, the total flow rate exiting the pin plate separator was designed to be evenly split between the upper and lower outlets. This flow-split was maintained by drawing the target outlet flow rate from the lower outlet and maintaining the upper outlet at atmospheric pressure. The same approach was also used in the matched flow case, where the outlet flow rates are set assuming 100% separations.

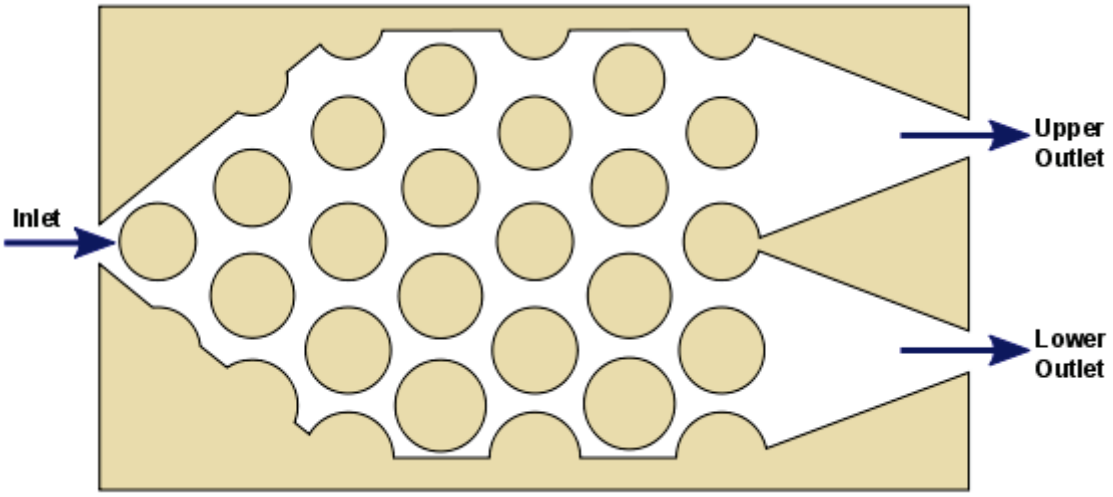

Figure 4.3. Boundaries in Pin Plate Separator.

4.4.2 Fluid and Model Properties

Fluid domain was simulated using the Lattice Boltzmann method on a grid with a node spacing of 12.5 μm and a time step of 361.7 ns. The water was assumed to have a kinematic viscosity of 1×10^{-3} m^2/s whereas the air was assumed to have a kinematic viscosity of 1.6×10^{-5} m^2/s. The air water surface tension was assumed to be 0.072 N/m and the contact angle ranged from 48° to 132°. Gravitational forces are assumed to not be present. Model parameters were determined from previously determined correlations shown in *Figure 4.4* through *Figure 4.6*.

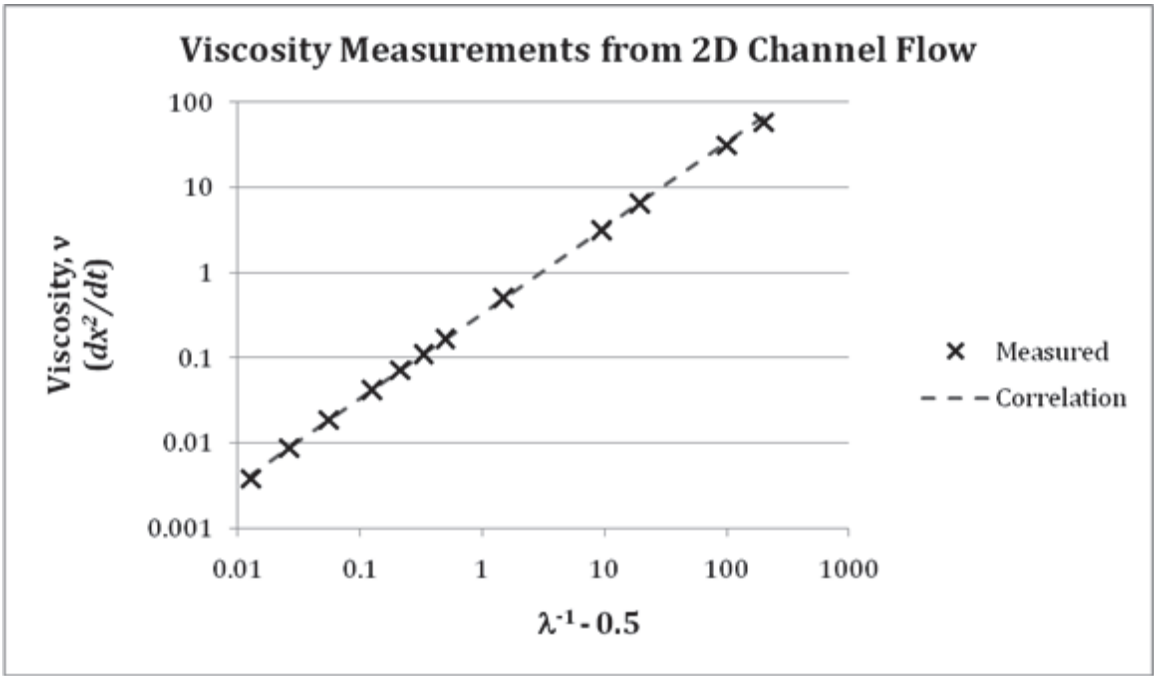

Figure 4.4. Relationship between kinematic viscosity and the fluid relaxation parameter, λ. The fluid relaxation parameter is a constant used directly in the Lattice Boltzmann model.

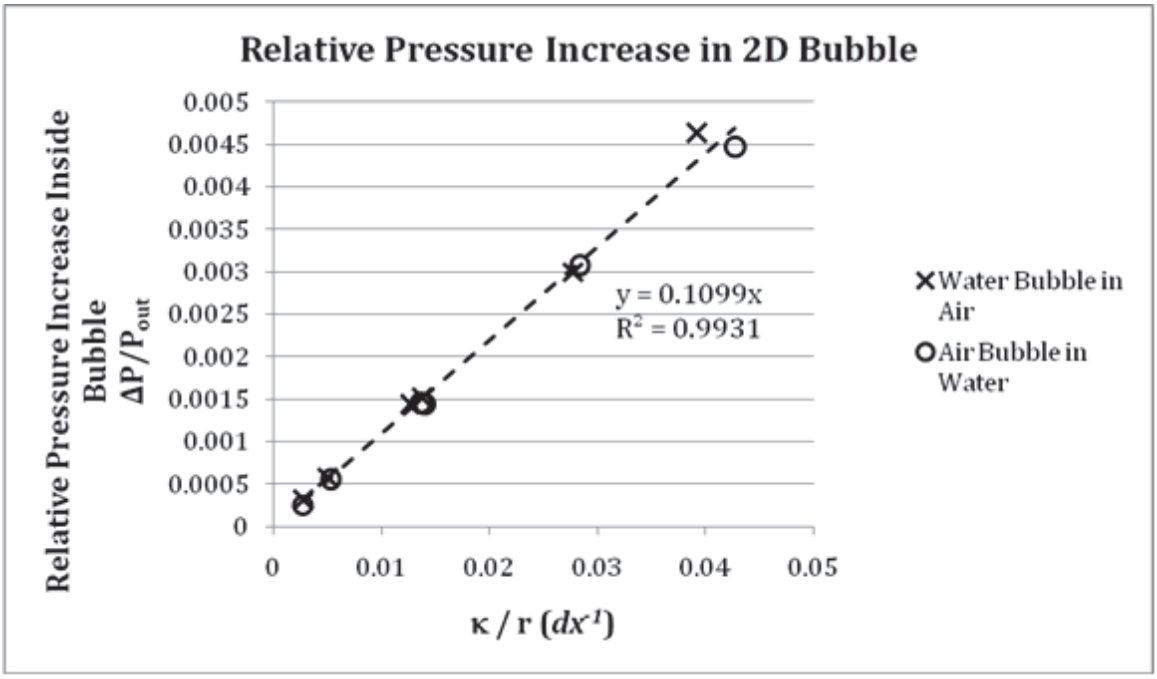

Figure 4.5. Correlation for determining the relationship between surface tension and the interfacial energy κ. The interfacial energy is a constant directly used in the Lattice Boltzmann model.

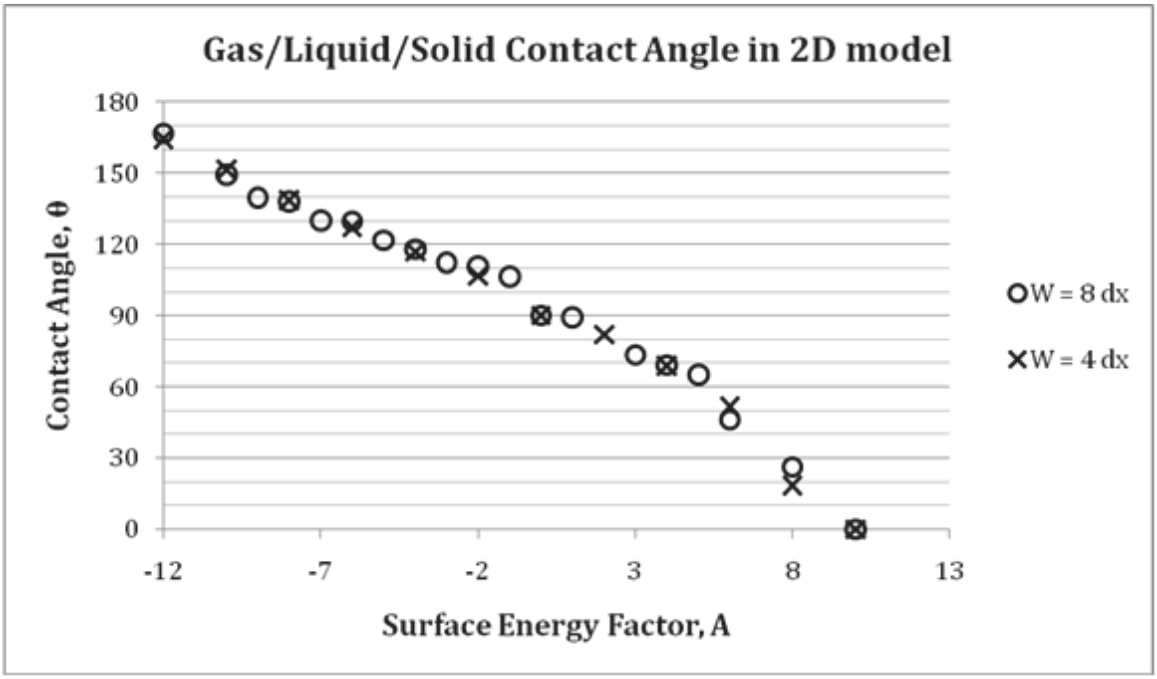

Figure 4.6. Correlation for determining the relationship between contact angle and the solid surface energy factor, A. The solid surface energy factor is used directly in the lattice Boltzmann model.

4.5 Simulation Results

A series of simulations were run to examine the effect of different design and operating parameters on the gas-liquid separation with the pin plate separator device. In each case, the separation efficiency was measured based on the flow of air out of the upper and lower outlets. In this work, the separation efficiency is defined as:

$$\text{Separation Efficiency} = \frac{[\text{Air flow through upper outlet}] - [\text{Air flow through lower outlet}]}{[\text{Total air flow}]}$$

In all cases, the measurements were made once a steady state flow of air and water out of the device was reached. In *Figure 4.7* airflow measurements from a simulation are shown as an example. In this case, 14.1% separation efficiency was calculated from the steady state slopes of the accumulated airflow leaving the upper and lower outlets.

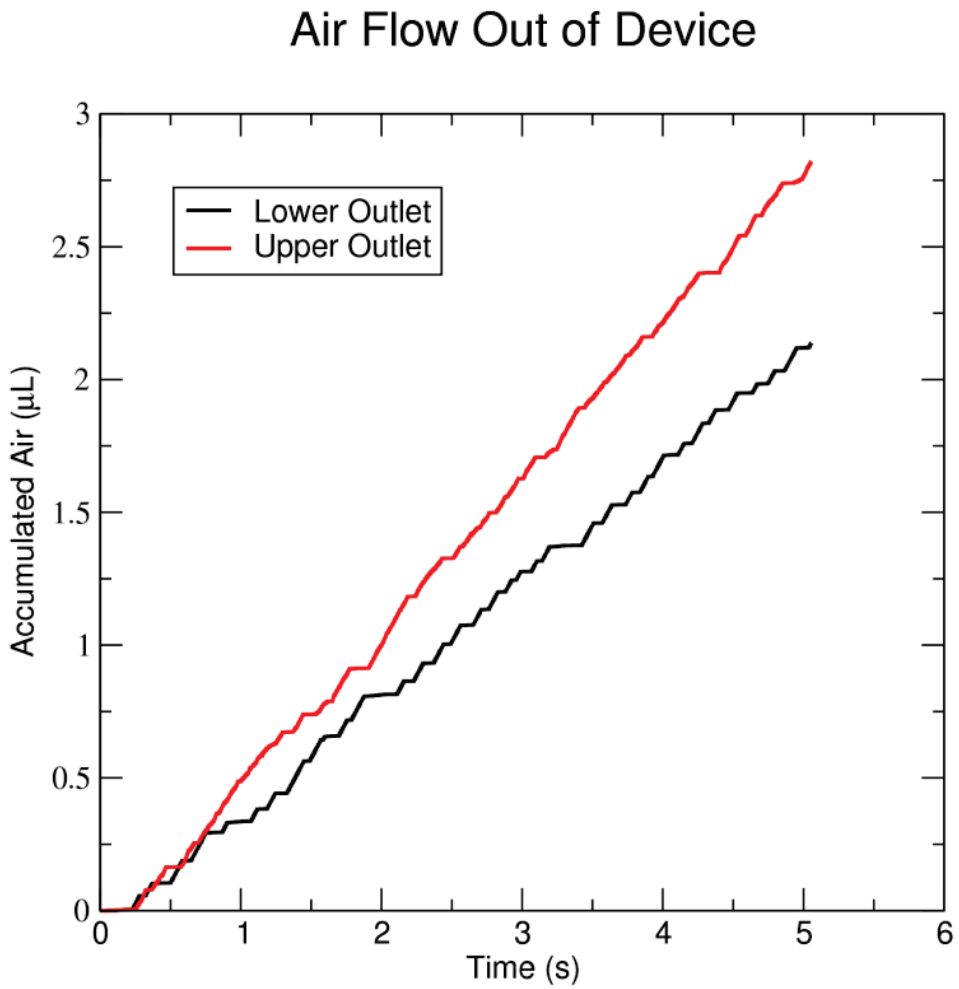

Figure 4.7. Total air flow from upper and lower outlet in geometry #1, total flow = 2 µL/s, gas-liquid-solid contact angle = 90°; air mix = 50%. 14.1% separation efficiency.

4.5.1 Effect of Flow Rate and Contact Angle

A series of simulations were run in the pin plate separator geometry #1 where the flow rates were varied between 1.0 µL/s and 3.0 µL/s and the gas-liquid-solid contact angle was varied from 48° to 132°. Snapshots from selected simulations are shown in *Figure 4.8* through *Figure 4.10*. The effect of the contact angle can be seen clearly in these figures by examining the gas-liquid-solid interfaces. In *Figure 4.8*, the results of simulations where the solids are modeled as being hydrophilic (contact angle of 48°) are shown. In this image, the liquid is attracted to the solid surfaces and the interfaces are shaped accordingly. In *Figure 4.9*, results of a simulation where the solid surface is

modeled as being neutral (contact angle of 90°) are displayed. As a result, at points of gas-liquid-solid contact, the interface approaches the solid surface at an angle normal to the surface. Finally, in *Figure 4.10* the results of a simulation where the surface is modeled as hydrophobic (contact angle of 132°) are displayed. In this case, the liquid is repelled from the surface at the point of gas-liquid-solid contact.

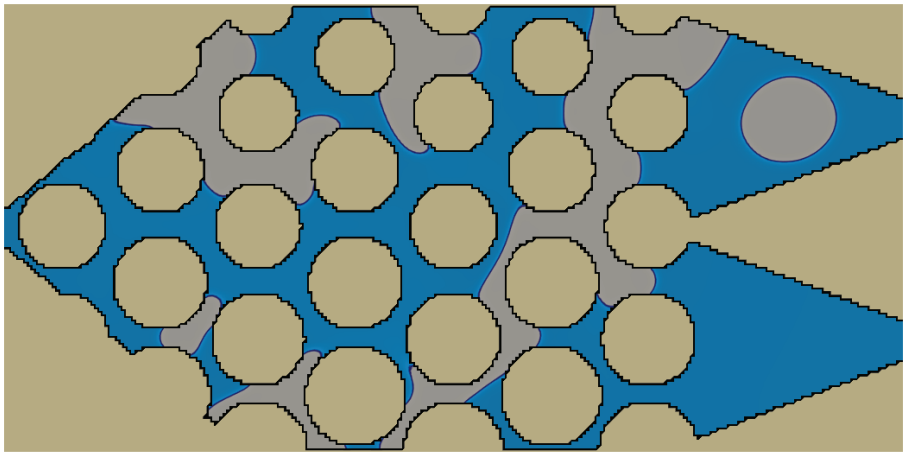

Figure 4.8. Snapshot from simulation in geometry #1, total flow = 2 µL/s, gas-liquid-solid contact angle = 48°; air mix = 50%. Water is shown in blue and air in gray.

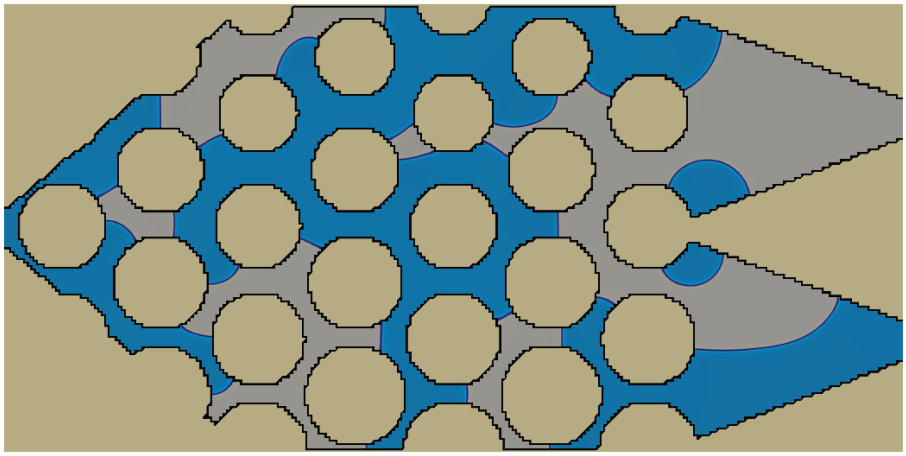

Figure 4.9. Snapshot from simulation in geometry #1, total flow = 2 µL/s, gas-liquid-solid contact angle = 90°; air mix = 50%. Water is shown in blue and air in gray.

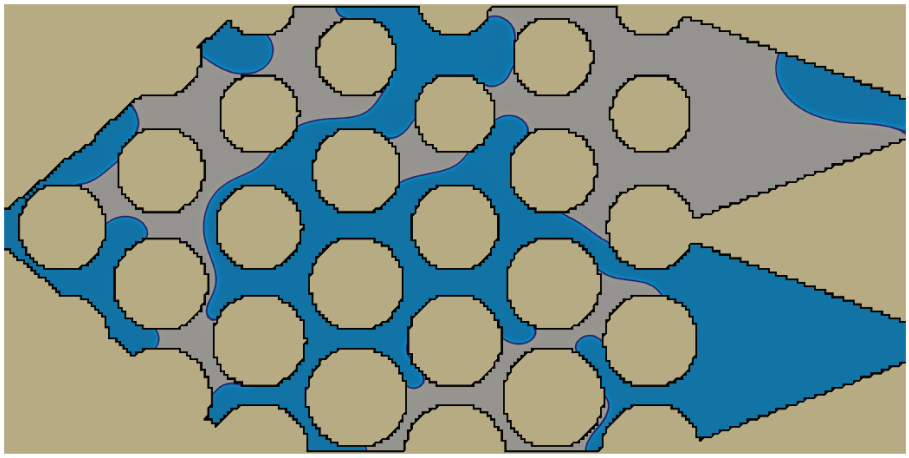

Figure 4.10. Snapshot from simulation in geometry #1, total flow = 2 µL/s, gas-liquid-solid contact angle = 132°; air mix = 50%. Water is shown in blue and air in gray.

The separation efficiencies for simulation in geometry #1 for flow rates of 1.0, 2.0, and 3.0 µL/s and contact angles of 48°, 90°, and 148° are shown in *Figure 4.11* (plotted as a function of flow rate) and in *Figure 4.12* (plotted as a function of contact angle). Overall, there is a tendency for the air to exit the upper outlet, regardless of the flowrate or contact angle in the simulation. Therefore, it would suggest that the capillary forces are not dominating in all cases within the flow. At 1.0 µL/s, however, the flow is slow enough that interfacial capillary forces can influence the separation.

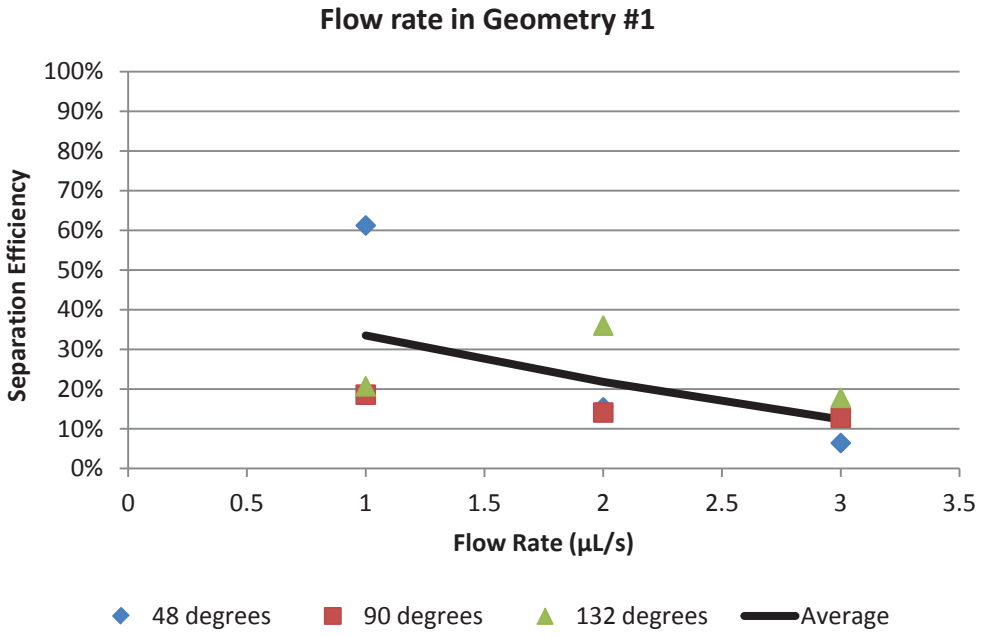

Figure 4.11. Results showing separation efficiency as a function of flow rate at gas-liquid-solid contact angles of 48°, 90°, and 132°. The feed was a 50:50 mix of air and water.

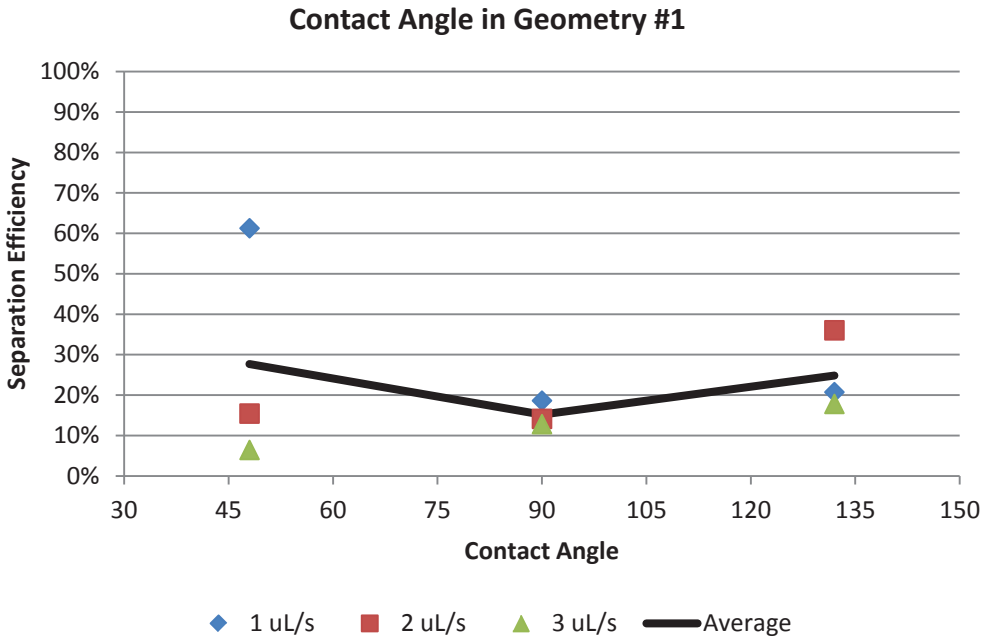

Figure 4.12. Results showing separation efficiency as a function of gas-liquid-solid contact angle for flow rates of 1.0, 2.0, and 3.0 µL/s. The feed was a 50:50 mix of air and water.

In the hydrophillic case (48° contact angle) at 1.0 μL/s, in which the capillary forces would drive the air to the upper outlet, a higher separation efficiency was observed than under other conditions. In the hydrophobic case at 1.0 μL/s, on the other hand, there continued to be air forced to the upper outlet even though the capillary forces would be driving the air to the lower outlet. Also of note is the fact that even a neutral surface (90° contact angle) was observed to create a separation of air. Therefore, it may be possible to design a pin plate separator in the future that does not require a hydrophobic or hydrophillic surface treatment.

4.5.2 Effect of Air mix and Pin Diameter Gradient

The amount of air in the fluid feeding the pin plate separator was also studied along with the effect of changing the pin gradient in the geometry. The amount of air, expressed as a percentage of the total flow, was varied from 25% to 75% in simulations whereas the gas-liquid-solid contact angle was constant at 90°.

In *Figure 4.13*, snapshots from these simulations are shown. These snapshots clearly show the difference between the stream being predominately water or predominately air. In *Figure 4.14*, the separation efficiencies are plotted as a function of the air mix for flow rates of 1.0 and 3.0 μL/s in geometries #1 and #2. At low air mixes, both geometries are performing well and looking at the average plots, we see that the higher pin gradient does indeed produce a stronger separation at 50% air mix or below. This is an important result because the pin gradient is the only feature being used to create the separation. For 75% air mix, however, a negative separation efficiency was observed in both geometries. This surpising result is discussed in the next section.

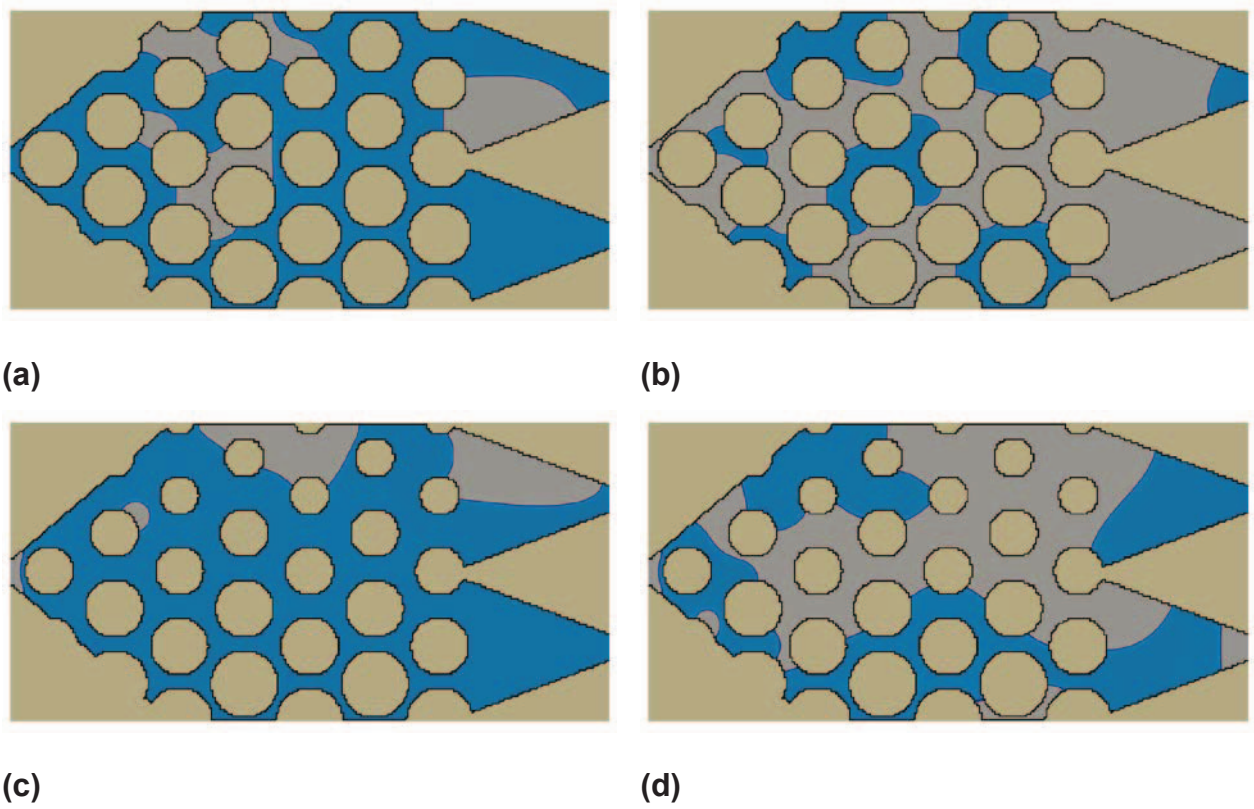

Figure 4.13. Snapshots of separation in pin plate geometries: (a) 25% air in geometry #1; (b) 75% air in geometry #1; (c) 25% air in geometry #2; (d) 75% air in geometry #2.

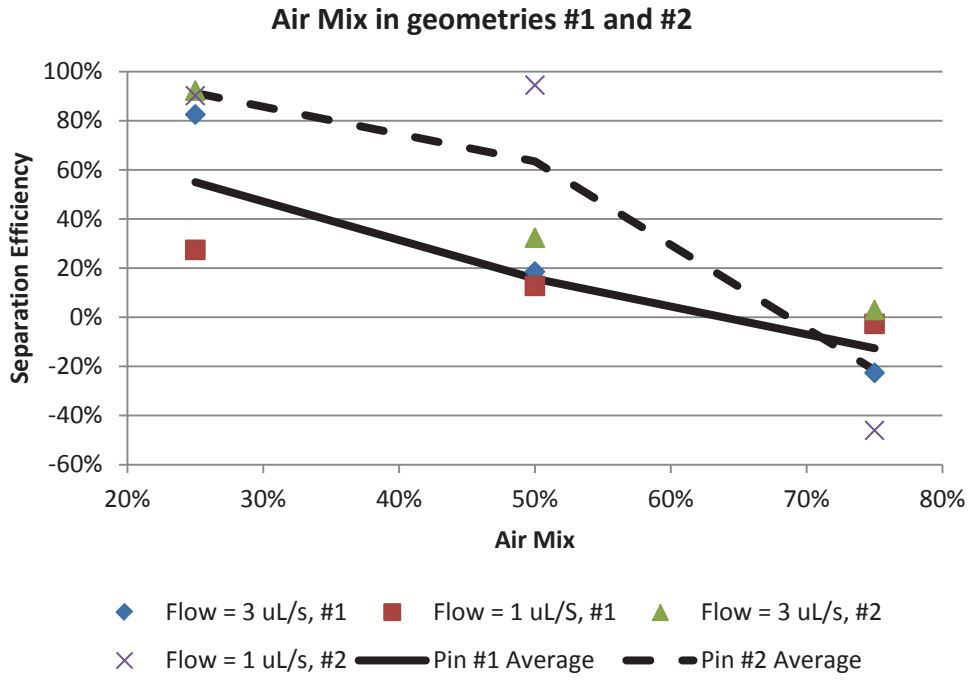

Figure 4.14. Results showing separation efficiency as a function of air mix in geometries #1 and #2 for flow rates 1.0 and 3.0 µL/s and contact angle of 90°.

4.5.3 Effect Total Outlet Flow Rates

As shown in *Figure 4.14*, a negative separation efficiency was observed for air mixes at 75% which means that more air is leaving the lower outlet than the upper outlet. One source of this could be that the upper and lower outlets were fixed to have equal total flow. Under this "equal" flow condition, perfect separation is not possible for a 75% air mix and for this reason, the "matched" outlet flow was studied. In a matched flow scenario, the total flow rates at the upper and lower outlets are adjusted as if 100% separation was occuring in the device. The matched flow splits are shown in *Table 4.2* along with the equal flow cases.

Table 4.2. Total flow out of upper / lower outlets for equal flow and matched flow cases.

Air Mix	Equal flow	Matched Flow
25%	50% / 50%	25% / 75%
50%	50% / 50%	50% / 50%
75%	50% / 50%	75% / 25%

Simulations were performed in geometry #2 to compare the matched flow and the equal flow cases, the results of which are shown in *Figure 4.15*. Switching the outlet from an equal flow to a matched flow did not affect the operation for air mixes at or below 50% but for the 75% case, the simulation showed a strong shift in performance.

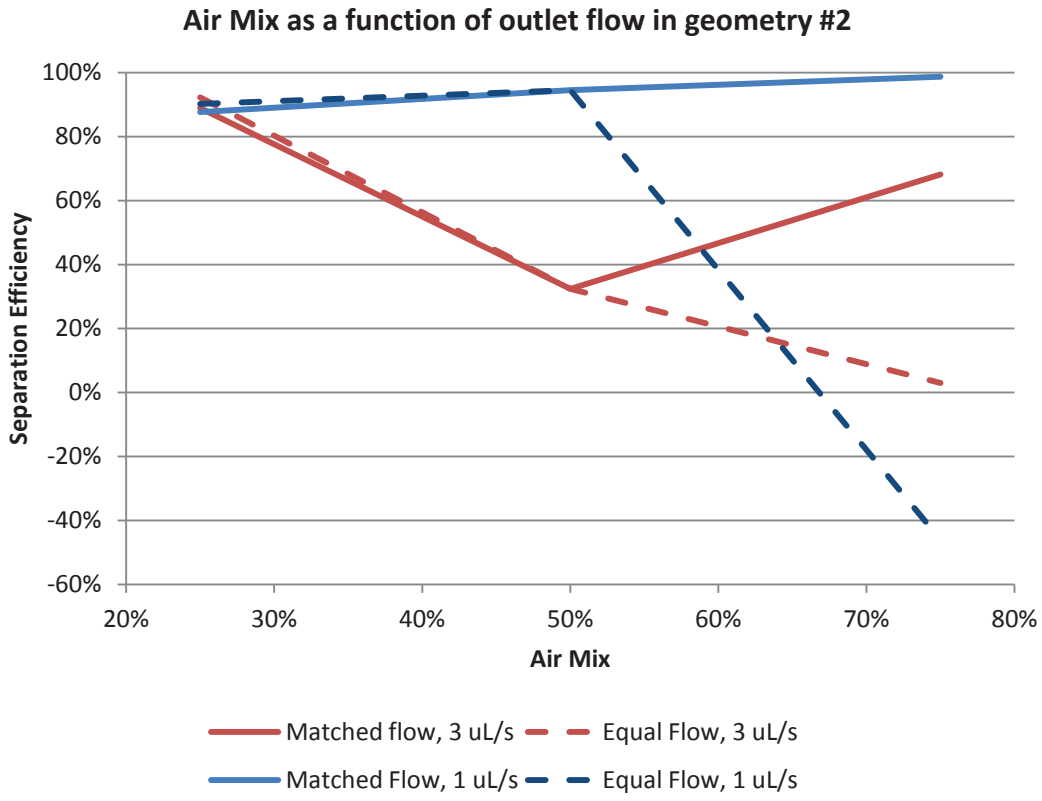

Figure 4.15. Results showing separation efficiency as a function of air mix in geometries #2 for flow rates 1.0 and 3.0 µL/s and contact angle of 90°. In the matched flow case, the total flow is set for 100% separation. In equal flow, total flow is evenly divided between upper and lower outlets.

At 1.0 µL/s of flow, the separation efficiency went from being strongly negative to being nearly perfect whereas the 3.0 µL/s simulation case went from a negligible amount of separation to a strong separation. Although these are only two data points, this is an interesting result. At a minimum, it highlights the importance that outlet flow control would likely play in the future development and operation of an efficient pin plate separator device.

4.6 Conclusions on Modeling Pin-Plate Separator with lattice Boltzmann method

The simulations of the small test geometries with the lattice Boltzmann method showed that the pin plate separator could indeed be an effective device for separating gas-liquid flows in microgravity conditions. At low flow rates, the air was being forced in part to the upper outlet and in these conditions it appeared that the capillary forces played a substantial role in creating the separation. However, these simulations also showed that the separation is not entirely dominated by capillary forces within the device and that the pin gradient is possibly creating a separation through other mechanisms as well. Finally, studies of the amount of air in the inlet and outlet streams showed that the device could perform well under a range of air mixes but that the outlet flow control may play an important role in achieving the separation. After observing these satisfactory results of the numerical simulation, a decision was made to produce an experimental test apparatus, which could serve to verify the feasibility of phase separation in a pin-plate design.

5.0 Experimental Verification of Two-Phase Separation in the Pin- Plate Separator

As suggested in the previous Section a Test-Loop was designed and manufactured to enable a feasibility study of the Pin-Plate operation. The purpose of this experimental apparatus was to provide evidences that a large size Pin-Plate could be designed, manufactured and successfully operated. *Figure 5.1* is a schematic representation of the Test-Loop.

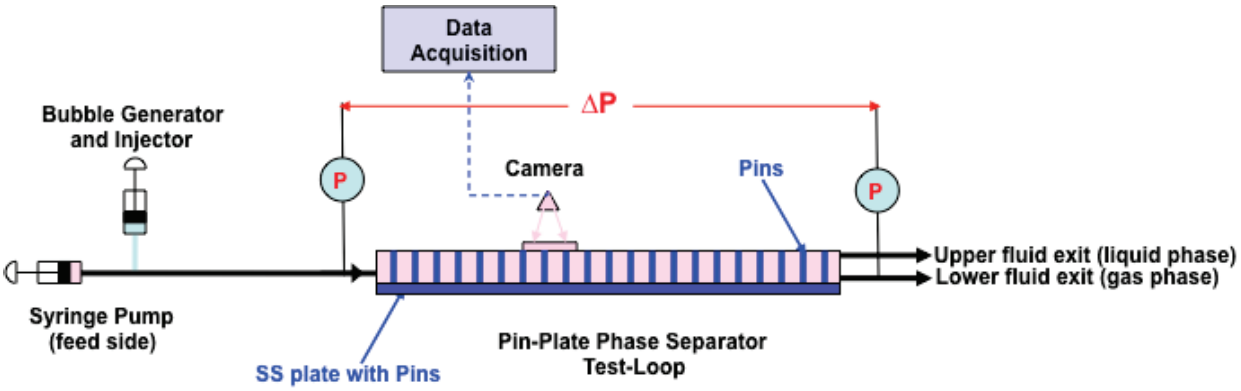

Figure 5.1. Schematic of the Test-Loop for phase separation testing with Pin-Plate.

5.1 Pin-Plate Design

A large Pin-Plate 9 x 12 cm in size is designed and manufactured out of SS shim 750 μm thick. Approximately 8000 cylindrical posts, 200 μm in height and 200-to-1000 μm in diameter, were placed in a triangular pattern as shown in *Figure 5.2*. The Pin-Plate was placed in a closed box made out of an aluminum base (bottom), and a Plexiglas (top), which enabled visual observation of gas (bubbles) and liquid motion between microposts. The Pin-Plate was produced by using photolithographic and chemical etching micromachining methods. In this feasibility study the surface of the Pin-Plate was not chemically treated for the adjustment of hydrophobicity/hydrophilicity of surfaces. *Figure 5.3* shows the 'exploded' view of the box and the Pin-Plate.

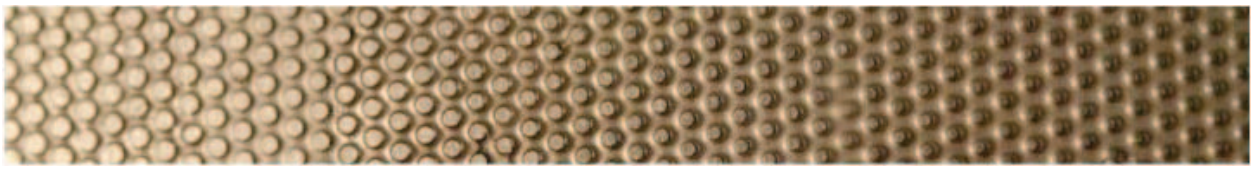

Figure 5.2. A photograph of a section of the Pin-Plate surface showing microposts arranged in a triangular pattern.

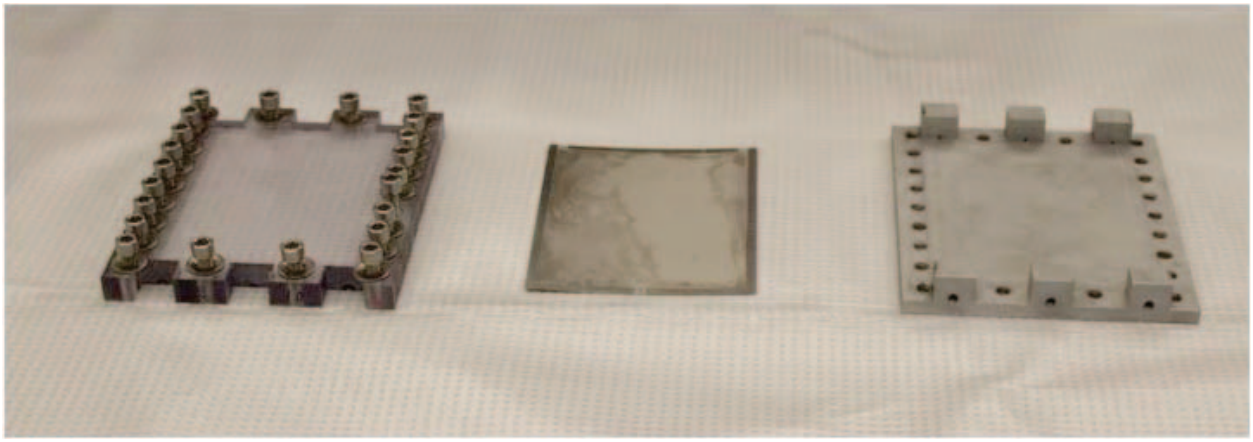

Figure 5.3. Exploded view of the box: top Plexiglas plate (left); stainless steel Pin-Plate (middle); and aluminum bottom plate (right).

Figure 5.4 illustrates the Pin-Plate positioned into the aluminum base. Discoloration marks on the plate are a consequence of SS oxidation (after chemical etching) with oxygen from air, which naturally and quickly dissolves in de-ionized water.

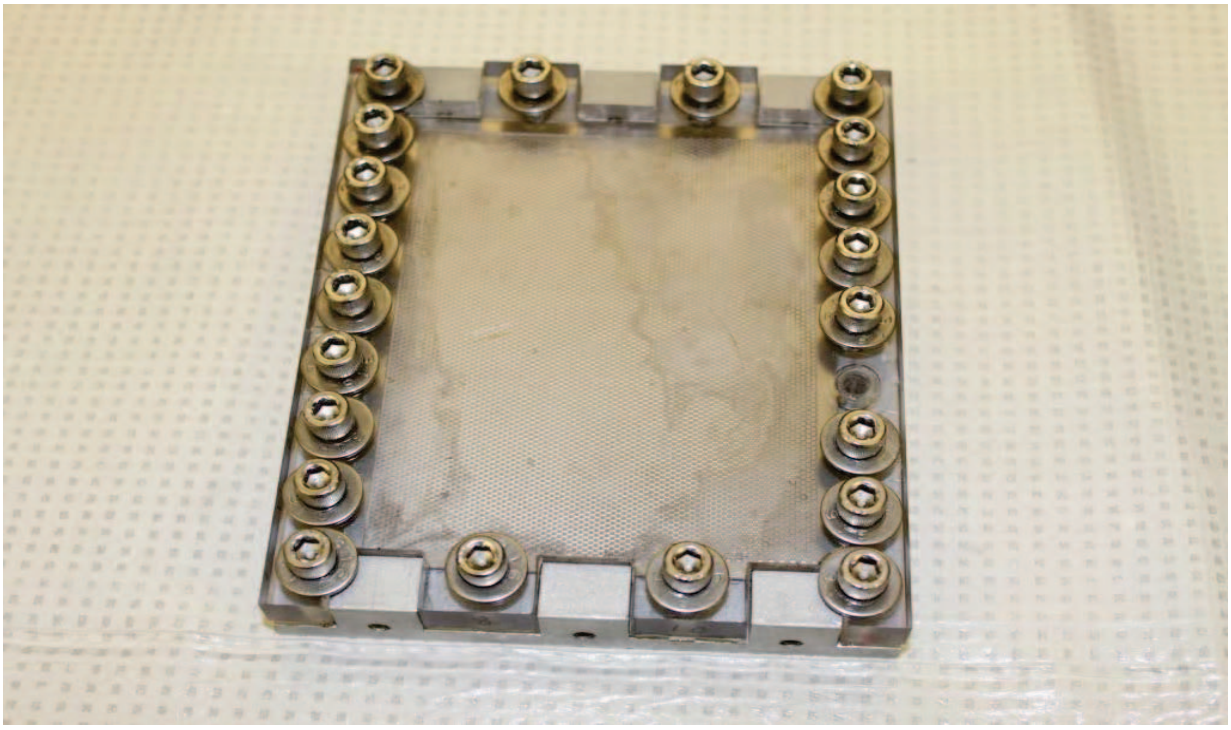

Figure 5.4. Assembled box with Pin-Plate below the Plexiglas top plate.

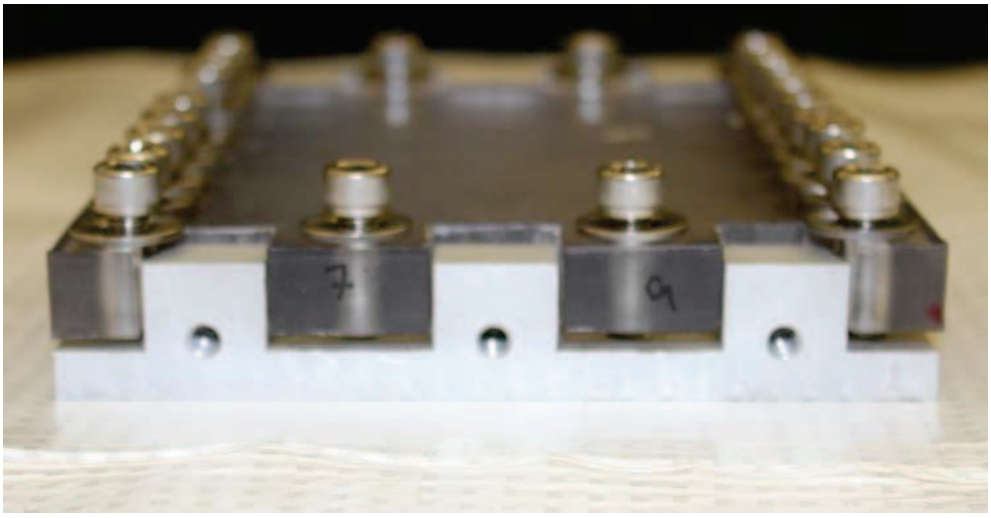

Figure 5.5. Side view of the assembled box with entrance/exit ports.

5.2 Bubble Size Control and Generation

Special attention was given to generation of bubbles (and control of bubble size), which were introduced into an inlet stream as shown in the schematic of the Test-Loop (*Figure 5.1*). We used a specially designed device, developed elsewhere, to generate bubbles with controlled frequency and size. The ability to introduce bubbles into an experimental apparatus under controlled conditions enabled us to study and record the motion of the bubbles as they progressed through the Pin-Plate. This will be particularly useful for any future quantitative study of the phase separation effects in the Pin-Plate. *Figure 5.6* shows the bubble generator which was acquired elsewhere.

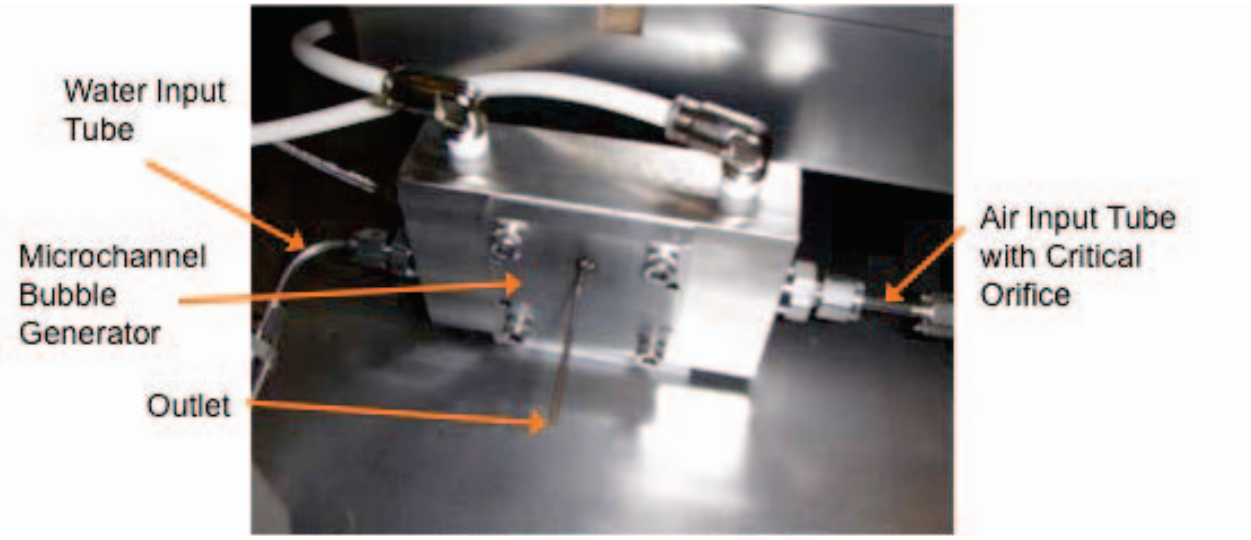

Figure 5.6. Bubble generator.

Figure 5.7 shows a train of bubbles in a capillary tube ready to be introduced into the main flow stream leading into the Pin-Plate. One should notice that bubbles could differ in size, although they are generated under identical conditions. Still, the predominant (nominal) size of bubbles is easily observed.

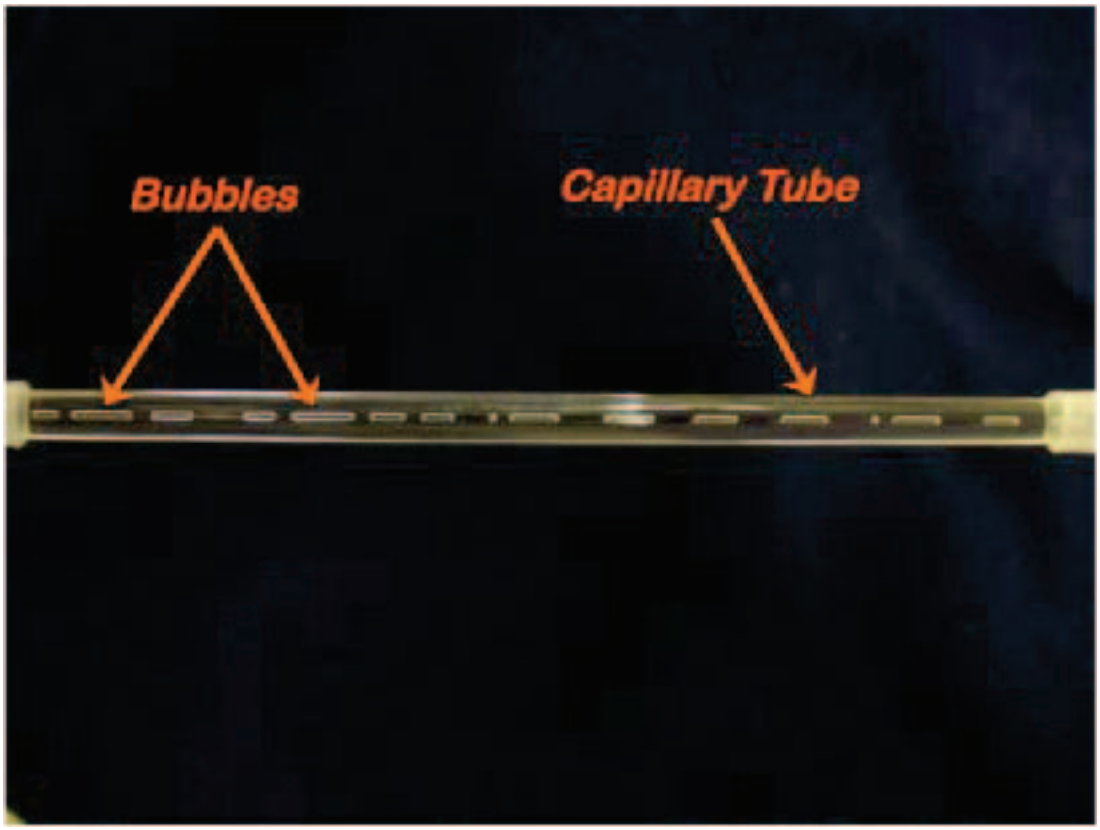

Figure 5.7. Bubbles generated and ready to be introduced into the Pin-Plate.

5.3 Pin-Plate Operation

As mentioned earlier in this section, the experimental study was conducted to confirm the basic conjecture that emerged from LB simulation; i.e., to confirm feasibility of gas-liquid phase separation based on the interface phenomena occurring in the Pin-Plate microstructure. While the fundamental phenomena involved in phase separation in the Pin-Plate are relatively simple and understandable, experimental demonstration of the anticipated phenomena is much more complex. Many secondary and tertiary effects, which are clearly not captured by the mathematical model, deserve fundamental consideration since they play noteworthy roles in actual operation of the Pin-Plate separator. These effects will be considered in more detail when we discuss the results of the feasibility study.

Bubble Motion and Separation

From all observations made in this study we can confidently conclude that the concept of the separation of the bubble phase (air) from the liquid phase (water stream) in the Pin-Plate is proven to be exceedingly successful. Almost all bubbles introduced through the middle-input port of the plate were directed, as anticipated, toward the single (side) exit port. This result seems to be more compelling than simulation results obtained with LB modeling. The time sequenced photos in *Figure 5.8* (viewed from left to right and top to bottom) clearly show the progression of a single (typical) bubble toward the anticipated exit port of the Pin-Plate. The bubble size was approximately 5 mm x 10 mm. All bubbles in this size ranged moved readily toward the edge of the Pin-Plate where posts were smaller, thus local curvature of the interface was smaller. Their motion was clearly influenced by local curvature (in-between two adjacent posts) of the interface. The velocity of the bubble was somewhat staggered reflecting discreet events of bubble migration resulting from disconnection of the bubble's interfaces at its tail end and the formation of new interface lines between the posts at the front of the bubble.

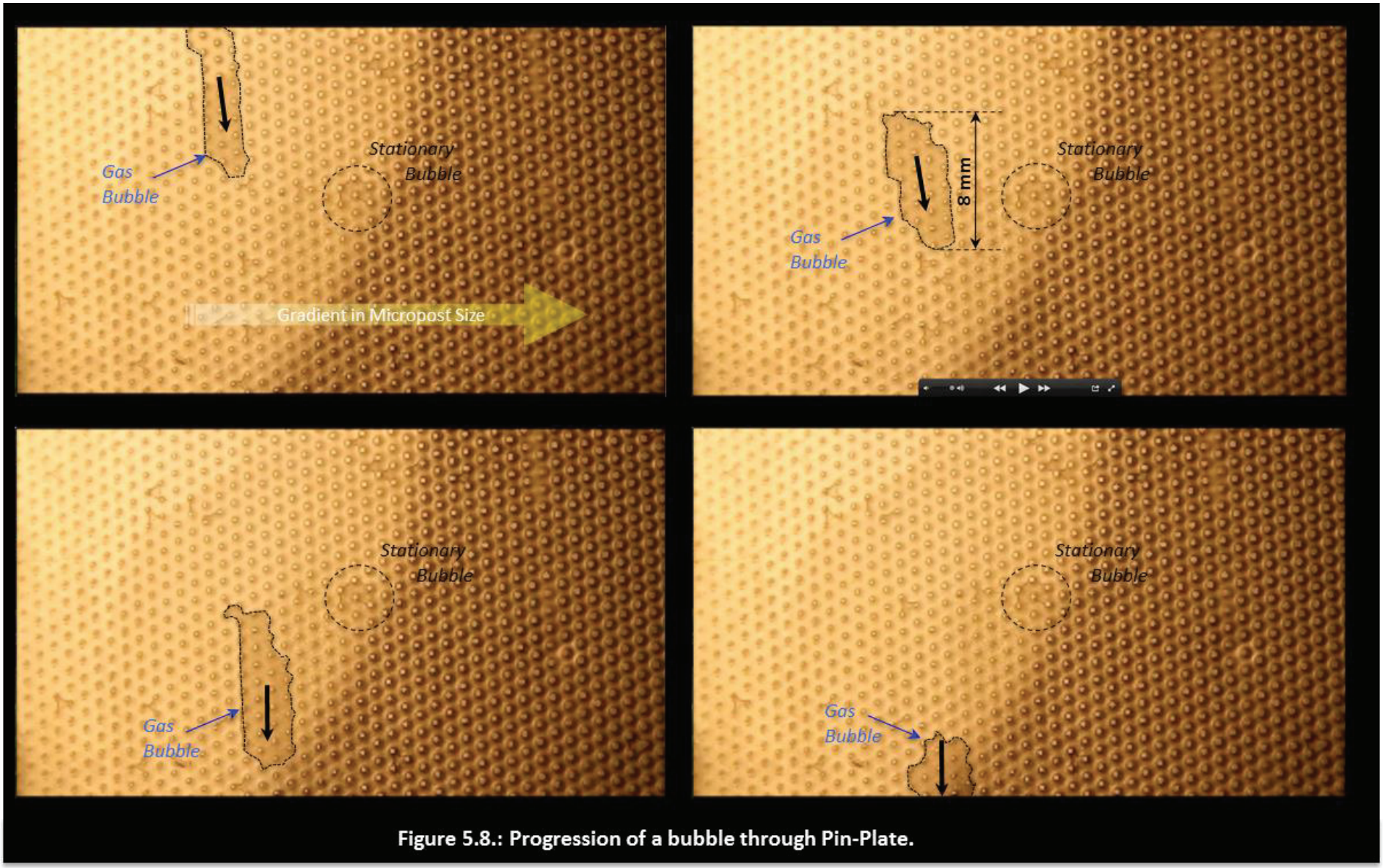

Figure 5.8.: Progression of a bubble through Pin-Plate.

Two secondary effects were observed during bubble motion between the inlet and exit ports:

1) The hydrophilicity of SS surface was not uniform/homogenous throughout the plate, thus sporadically creating different contact angles between the gas-liquid interface and micropost surfaces. This seemed to be noticeable only when the bubble's motion was intermittently retarded; but eventually the dominant forces would overcome this local retardation.

2) The bottom part of the Pin-Plate was not flat due to the nature of the chemical etching process used to micromachine the plate. The space in-between microposts at the bottom of the plate was rather oblong (hemispherical) while the top, Plexiglas, plate provided a rather flat surface. This geometrical inconsistency results in different local curvature of the interface than nominally expected and represented in the mathematical model.

Critical Bubble Size

Figure 5.7 shows that occasionally the bubble generator would create very small bubbles. These small bubbles would appear to be approximately 1 mm in size once they entered the Pin-Plate space. Initially they would move in the correct direction until they enter the region of smaller pins with wider inter-post spaces. At these locations small bubbles stand a reasonably high chance of being "arrested" in-between neighborhood posts. One of these bubbles is clearly visible on all four frames shown in *Figure 5.8*. These bubbles would not move unless a much larger bubble would pass by and coalesce with them into an even larger bubble. Thus, it appears that bubbles smaller than, or approximately equal to the size of the inter-post space would most probably be arrested in the plate until coalescence occurs. It is fortunate that small bubbles become trapped until they coalesce with other bubbles because this phenomenon prevents them from migrating until they are sufficiently large to be directed by capillary action to the desired port. Because small bubbles are prevented from migrating, it is anticipated that small bubble introduction and bubble coalescence will attain a steady state. As such, small bubbles will not accumulate to the point where they interfere with the operation of the separator. Only bubbles smaller than the gap

between posts can elude capture. The formation of ultra-small bubbles, however, is not energetically favorable so their occurrence is not to be expected under common conditions.

Bubble Coalescence

One somewhat unexpected discovery, both in LB simulation and visual observations was related to bubble coalescence. As bubbles move through the plate they tend to coalesce if an opportunity is created such that two adjacent bubbles touch each other. It seems that a curved interface in-between microposts reduces the energy of activation usually needed for the coalescence of bubbles. This tendency results in occasional formation of very large bubbles occupying substantial part of the plate, which creates disruptive fluid dynamic behavior. However, these large bubbles did not demonstrate any tendency to stay motionless in the plate. Rather, they quickly processed through the plate and passed through one of the exit ports. The only drawback created by large bubbles was substantial disruption of pressure distribution within the plate, which typically reduced the effectiveness of phase separation. Large bubbles were “happy” to leave the plate through the “designated” exit port: but, could cause other smaller bubbles to move in an unexpected direction. *Figure 5.9* shows one such large bubble, which formed through a series of bubble coalescence events, on the right side of the plate.

One additional secondary effect was observed during bubble coalescence. Smaller “debris” bubbles were often observed as leftovers following the coalescence of two larger bubbles. These ”debris” bubbles resemble small motionless trapezoids which form between adjacent posts with typical features of the stationary bubble identified in *Figure 5.8*. These small bubbles are readily swept away (coalesced) by the next large bubble that passes by. Interestingly the formation of these large bubble leftovers did not show up in our numerical simulation.

In conclusion: qualitative experimental evidence confirms that the concept of phase separation in the Pin-Plate, which is fundamentally based on the interface phenomena, fluid properties, and microscale architectural characteristics is viable. However, separation phenomena are rather complex, and secondary and tertiary

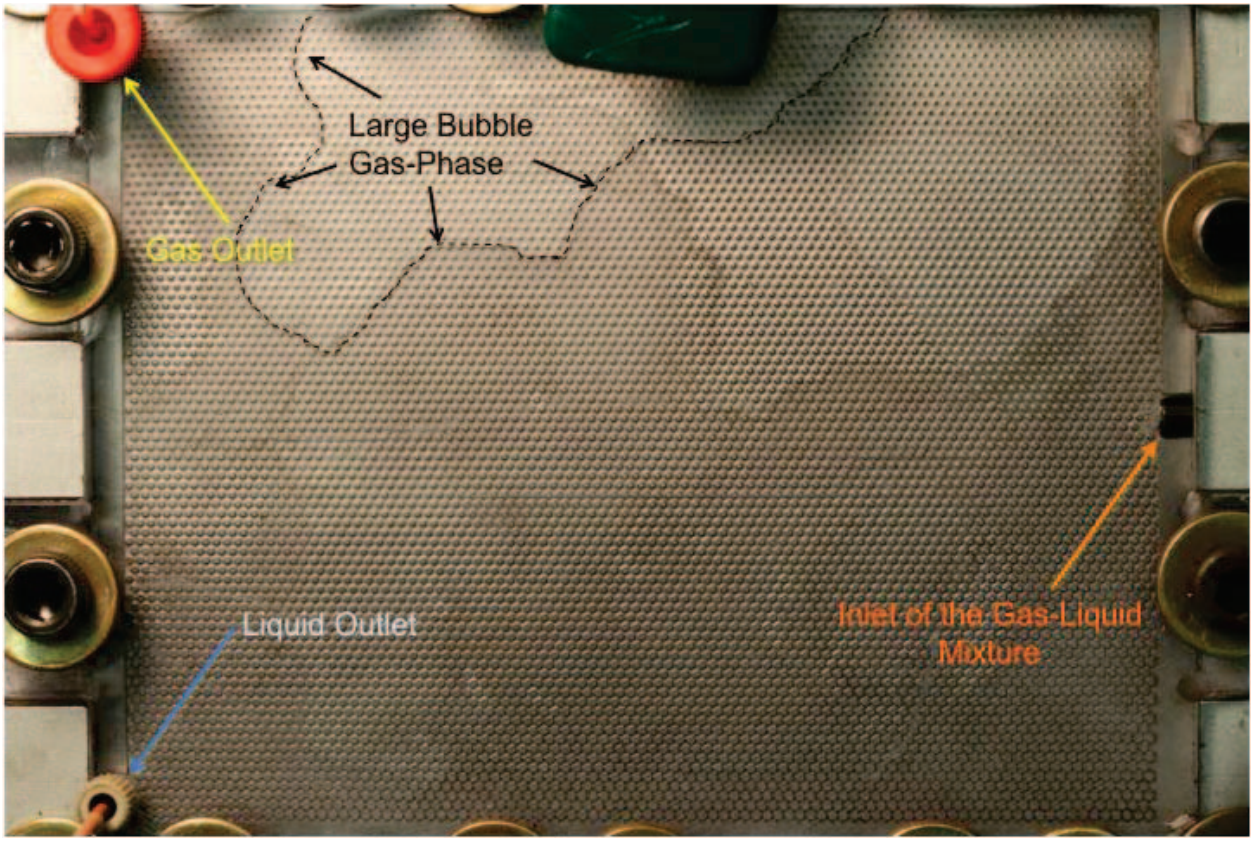

Figure 5.9. Large bubble formed on the side of the plate with gas exit port.

effects (typically not represented in mathematical model or design parameters) may seriously disrupt the operation of the Pin-Plate in its current design. Further investigation is needed, in which all system variables are controlled. This may lead to a new and innovative design of the Pin-Plate phase separator.

Subject Inventions

This NRA grant was for follow-on development of a new technology that was originally reported under NASA/MSFC SBIR contract NNM06AA47C entitled "Microgravity Compatible Gas-Liquid Separation using Capillary Pressure Gradients". The NASA New Technology ID number is 5021657. There is no additional new technology to report under this grant. This information is provided pursuant to Provision 1260.28 of the NASA Grant and Cooperative Agreement Handbook.

Summary of Research

This 3-year research effort has culminated in the design and testing of a zero-g demonstration prototype. Both the hydrophilic (glass) and hydrophobic (Teflon) media Capillary Pressure Gradient (CPG) cartridges prepared during the second year's work were evaluated. Results obtained from ground testing at 1-g were compared to those obtained at reduced gravities spanning Martian (1/3-g), Lunar (1/6-g) and zero-g. These comparisons clearly demonstrate the relative strength of the CPG phenomena and the efficacy of its application to meet NASA's unique gas-liquid separation (GLS) requirements in non-terrestrial environments.

LB modeling software was concurrently developed during this work to accurately simulate the observed CPG driven gas-liquid separation. The design and fabrication of a micropost plate-lamina HS cell structure was also performed which served as a computationally attainable geometric structure facilitating direct comparison between physical phenomena observed in our laboratory and the LB software predictions.

Based upon the successful proof of concept work reported herein, further development of CPG based phase separation phenomena and the corresponding novel Lattice Boltzmann computer modeling approach is highly recommended. Not only were we able to demonstrate CPG separation of mixed air-water streams while operating in 180° opposition to gravity environs from zero-g up to and including 1-g using relatively coarsely layered particle gradient devices, but a unique theoretical model/simulation approach was also developed which permits effective tracking of gas/liquid phase boundaries via application of the fundamental physical/material properties of the solid, liquid and gas participants within a pin-plate cell 2-D geometric structure. Future work would focus on the further development of these technologies towards the ultimate goal of performing an ISS flight experiment.

REFERENCES

1. Parker, J.M. A Novel Lattice Boltzmann Method for Treatment of Multicomponent Convection, Diffusion, and Reaction Phenomena in Multiphase Systems, Thesis, Oregon State University Thesis, Corvallis, 2008.
2. Parker, J.M., and Jovanovic, G.N., A Lattice Boltzmann Model for Multiphase Equilibrium in Convection-Diffusion-Reaction Chemical Processes, presented at International Conference on Mesoscopic Methods in Engineering and Science, Munich, 2007.
3. Parker, J.M., and Jovanovic, G.N., Lattice Boltzmann Modeling of Multicomponent Systems with Chemical Potential Driven Molecular Diffusion, presented at International Conference on Mesoscopic Methods in Engineering and Science, Amsterdam, 2008.
4. Holtsnider, J.T. and Atwater, J.E., Microgravity Compatible Capillary Pressure Gradient Based Gas-Liquid Separator, UMPQUA Research Co., Final Report, contract NNM06AA47C, NASA-MSFC, 2006.
5. Microchannel Dialyzer Development – Supplemental GAP-Fund Project; Final Technical Report, Oregon State University, May 2009.
6. Parker, J.M., Jovanovic, G.N., Wheeler, R.R. and Duval, W.M., Lattice-Boltzmann Model Development For Capillary Pressure Gradient Gas/Liquid Phase Separation in Microgravity, AIAA paper 2011-5196, presented at the 41st International Conference on Environmental Systems, Portland, 2011.